

MID1-COMPLEMENTING ACTIVITY regulates cell proliferation and development via Ca²⁺ signaling in *Marchantia polymorpha*

Megumi Iwano,^{1,*} Noriyuki Suetsugu,^{2,†} Ryuichi Nishihama,³ Sakiko Ishida,¹ Tomoaki Horie,⁴ Alex Costa,⁵ Tatsuya Katsuno,⁶ Midori Kimura,⁷ Kazuko Iida,⁷ Hidetoshi Iida,⁷ Takeharu Nagai,⁸ Takayuki Kohchi^{1,*}

¹Graduate School of Biostudies, Kyoto University, Kyoto 606-8502, Japan

²Department of Life Sciences, Graduate School of Arts and Sciences, The University of Tokyo, Tokyo 153-8902, Japan

³Department of Applied Biological Science, Faculty of Science and Technology, Tokyo University of Science, Noda, Chiba 278-8510, Japan

⁴Division of Applied Biology, Faculty of Textile Science and Technology, Shinshu University, Ueda, Nagano 386-8567, Japan

⁵Department of Biosciences, University of Milan, Milano 20133, Italy

⁶Graduate School of Medicine, Kyoto University, Kyoto 606-8501, Japan

⁷Department of Biology, Tokyo Gakugei University, Koganei, Tokyo 184-8501, Japan

⁸SANKEN, The University of Osaka, Ibaraki, Osaka 567-0047, Japan

*Author for correspondence: iwano.megumi.5r@kyoto-u.ac.jp (M.I.), tkohchi@lif.kyoto-u.ac.jp (T.K.)

†These authors contributed equally to this work.

The authors responsible for distribution of materials integral to the findings presented in this article in accordance with the policy described in the Instructions for Authors (<https://academic.oup.com/plphys/pages/General-Instructions>) are Megumi Iwano (iwano.megumi.5r@kyoto-u.ac.jp) and Takayuki Kohchi (tkohchi@lif.kyoto-u.ac.jp).

Abstract

MID1-COMPLEMENTING ACTIVITY (MCA) is a land plant-specific, plasma membrane protein, and Ca²⁺ signaling component that responds to exogenous mechanical stimuli, such as touch, gravity, and hypotonic-osmotic stress, in various plant species. MCA is essential for cell proliferation and differentiation during growth and development in rice (*Oryza sativa*) and maize (*Zea mays*). However, the mechanism by which MCA mediates cell proliferation and differentiation via Ca²⁺ signaling remains unknown. Here, we address this question using the liverwort *Marchantia polymorpha*. We show that the *M. polymorpha* MCA ortholog, MpMCA, is highly expressed in actively dividing regions, such as apical notches in the thalli and developing gametangiophores, and that MpMCA is a plasma membrane protein. In vivo, Ca²⁺ imaging using a Ca²⁺ sensor (yellow cameleon) revealed that MpMCA is required for maintaining proper [Ca²⁺]_{cyt} levels in the apical notch region, egg cells, and antheridium cells. *Mpmca* mutant plants showed severe cell proliferation and differentiation defects in the thalli, gametangiophores, and gametangia, resulting in abnormal development and unsuccessful fertilization. Furthermore, expression of the Arabidopsis MCA1 gene complemented most of the defects in the growth and development of the *Mpmca* mutant plants. Our findings indicate that MpMCA is an evolutionarily conserved Ca²⁺-signaling component that regulates cell proliferation and development across the life cycle of land plants.

Introduction

Calcium ions are central regulators of physiological responses such as cell proliferation, growth, development, reproduction, and stress responses (Rasmussen 1970; Hepler 2005; Chen et al. 2015; Edel et al. 2017). In general, the cytosolic calcium ion concentration ([Ca²⁺]_{cyt}) is maintained at the submicromolar level (Berridge et al. 2000; Luan and Wang 2021). Various developmental and environmental signals trigger changes in [Ca²⁺]_{cyt} in plants. When plants are exposed to environmental stresses, such as low temperature, drought, salinity, and wounding, they trigger the elevation of [Ca²⁺]_{cyt} by influx from outer Ca²⁺ stores or release from inner Ca²⁺ stores (e.g. endoplasmic reticulum [ER] and vacuoles) and evoke downstream responses (reviewed in Resentini et al. 2021) including protection from various stresses and adaptation to new environmental conditions (Edel et al. 2017).

However, the fundamental role of Ca²⁺ signaling pathways in plant growth and development remains largely unknown.

Several cation-channel protein families in land plants have been studied as a Ca²⁺-permeable channel, including cyclic nucleotide-gated channel (CNGC) (Kaplan et al. 2007), glutamate receptors-like channel (GLR) (Simon et al. 2023), reduced hyperosmolality-induced [Ca²⁺]_{cyt} increase channel (OSCA) (Yuan et al. 2014), Piezo mechanosensitive ion channel (PIEZO) involved in root mechanotransduction (Mousavi et al. 2021), and two-pore channel (TPC1) (Furuichi et al. 2001). The model plant *Arabidopsis thaliana* (Arabidopsis) has 20 CNGC, 20 GLR, 15 OSCA, two PIEZO, and one TPC genes. Plasma membrane-localized CNGCs are required for pollen tube growth in Arabidopsis (Gao et al. 2016) and pathogen-associated molecular pattern (PAMP)-triggered Ca²⁺ signaling, which is critical for Ca²⁺-based immunity (Tian et al. 2019). GLRs are involved in pollen

Received June 21, 2024. Accepted October 11, 2024.

© The Author(s) 2024. Published by Oxford University Press on behalf of American Society of Plant Biologists.

This is an Open Access article distributed under the terms of the Creative Commons Attribution-NonCommercial-NoDerivs licence (<https://creativecommons.org/licenses/by-nc-nd/4.0/>), which permits non-commercial reproduction and distribution of the work, in any medium, provided the original work is not altered or transformed in any way, and that the work is properly cited. For commercial re-use, please contact reprints@oup.com for reprints and translation rights for reprints. All other permissions can be obtained through our RightsLink service via the Permissions link on the article page on our site—for further information please contact journals.permissions@oup.com.

tube growth and guidance (Michard et al. 2011), self-incompatibility responses (Iwano et al. 2015), and long-distance Ca^{2+} -based plant defense signaling (Mousavi et al. 2013; Toyota et al. 2018; Grenzi et al. 2023). Arabidopsis OSCA1 functions in Ca^{2+} signaling induced by hyperosmotic stress (Yuan et al. 2014). TPC is localized in the vacuolar membrane and regulates the conductance of both mono- and divalent cations (Kintzer and Stroud 2016). However, the mutant phenotypes of these Ca^{2+} channels are mild under unstressed conditions; thus, the involvement of these Ca^{2+} channels in plant cell proliferation during growth and development remains to be determined.

The MID1-COMPLEMENTING ACTIVITY (MCA) gene *AtMCA1* (At4g35920) was originally identified through Arabidopsis cDNA library screening based on the functional complementation of a yeast *Saccharomyces cerevisiae* *mid1* mutant defective in both Ca^{2+} influx and cell viability maintenance during exposure to mating pheromones (Nakagawa et al. 2007). Mid1 is a putative Ca^{2+} -permeable stretch-activated channel component and cooperates with a voltage-gated Ca^{2+} channel $\alpha 1$ subunit Cch1 (Kanzaki et al. 1999). However, *AtMCA1* is not homologous to Mid1 and regulates Ca^{2+} uptake in a Cchl-independent manner unlike Mid1 (Nakagawa et al. 2007). Arabidopsis has a paralog of *AtMCA1*, i.e. *AtMCA2* (At2g17780), with 73% amino acid sequence identity (Nakagawa et al. 2007). The Arabidopsis *Atmca1* mutant showed an impaired touch response in the primary roots (Nakagawa et al. 2007), and hypo-osmotic stress-induced Ca^{2+} uptake was observed in Arabidopsis roots overexpressing *AtMCA1* (Nakagawa et al. 2007). Ca^{2+} uptake activity in *Atmca2* mutant roots was lower than that in wild-type or *Atmca1* mutant (Yamanaka et al. 2010). Furthermore, the expression of *AtMCA1* enhanced mechano-sensitive channel activity in Chinese hamster ovarian cells (Nakagawa et al. 2007) and *Xenopus* oocytes (Furuichi et al. 2012). Experiments on liposomal membranes showed that the N-terminal regions of *AtMCA1* and *AtMCA2*, 173 amino acid residues each of the total length of 421 and 416, respectively, were sufficient for Ca^{2+} -permeability, and *AtMCA2* was sufficient for mechanosensitivity (Yoshimura et al. 2021). However, the structural features of *AtMCA2* elucidated by cryo-electron microscopy show no similarity to those of any characterized ion channels or membrane-bound transporters (Shigematsu et al. 2014; Hamilton et al. 2015), suggesting that MCAs are structurally unique ion channels.

MCA genes are involved in growth, development, and stress responses in rice and maize. In rice, RNAi of *OsMCA1* resulted in growth defects and late flowering in transgenic plants and reduced cell proliferation in cultured cells (Kurusu et al. 2012a). Mutations in *OsMCA1* resulted in severe dwarf phenotypes (Liu et al. 2015; Liang et al. 2020). The overexpression of tobacco (*Nicotiana tabacum*) *NtMCA1* and *NtMCA2* changes the proliferation rate of BY-2 cells in a Ca^{2+} concentration-dependent manner (Kurusu et al. 2012b). Furthermore, a *Zea mays* MCA ortholog CELL NUMBER REGULATOR13 (called *ZmMCA* for clarity), was discovered via molecular genetic analysis of *narrow odd dwarf* (*nod*) mutant that displayed severe growth and developmental defects attributable to impaired cell proliferation (Rosa et al. 2017). *ZmMCA* complemented the yeast *mid1* mutant but did not display detectable Ca^{2+} channel activity in *Xenopus* oocytes (Rosa et al. 2017). Although these studies suggest that MCA is a candidate gene for the Ca^{2+} signaling pathway that regulates plant growth and development, how MCAs function in cell proliferation and development during growth and development in individual plants remains unclear.

We used a model bryophyte, the liverwort *Marchantia polymorpha*, to further characterize MCAs as Ca^{2+} signaling components in plant cell proliferation (Ishizaki et al. 2008; Bowman et al. 2022). The

lineages of bryophytes and vascular plants diverged from the common ancestors of land plants. *M. polymorpha* is a dioicous species with separate male and female haploid individuals. Under white-light conditions, both female and male gametophytes grow continuously and perform asexual reproduction by generating gemma cups. Under long-day conditions, far-red light (FR) irradiation induces sexual reproduction (Chiyoda et al. 2008; Kubota et al. 2014). In female gametophytes, archegoniophores with archegonia that produce egg cells emerge from the apical notch region of the thalli, whereas antheridiophores with antheridia that produce sperm emerge in male gametophytes (Kohchi et al. 2021). In *M. polymorpha*, several small molecules involved in cell proliferation and development have been identified (Shinkawa et al. 2022; Hatada et al. 2023; Varshney and Gutjahr 2023), but the role of Ca^{2+} signaling in growth and development remains unknown. In such a scenario, an in vivo study of Ca^{2+} dynamics in *M. polymorpha* would be extremely advantageous for understanding the relationship between Ca^{2+} signaling and gene function in both vegetative growth and sexual reproduction across the life cycle.

In this study, we analyzed the function of the *M. polymorpha* MCA ortholog *MpMCA*. We characterized genome-edited lines for *MpMCA* and performed Ca^{2+} imaging using transgenic lines expressing a Ca^{2+} sensor protein to examine whether *MpMCA* is involved in the Ca^{2+} signaling pathway that functions in proliferation and reproduction. Our findings indicated that *MpMCA* plays pivotal roles in cell proliferation and development, possibly via the regulation of $[\text{Ca}^{2+}]_{\text{cyt}}$ during both vegetative growth and sexual reproduction.

Results

M. polymorpha has a single MCA ortholog *MpMCA*

We identified a single MCA ortholog, *MpMCA* (Mp5g19510), in the genome database of *M. polymorpha* (MarpolBase ver. 6: <https://marchantia.info>). *MpMCA* cDNA (Mp5g19510.1) encoded a polypeptide of 482 amino acid residues (Fig. 1A). The predicted *MpMCA* protein showed 39.5% and 38.7% amino acid sequence identity with *AtMCA1* and *AtMCA2*, respectively (Fig. 1B). As is the case with MCA proteins from other plant species, *MpMCA* has a single putative transmembrane segment near the N-terminus, an EF-hand-like motif on the N-terminal side, slightly beyond the middle region, a coiled-coil motif in the middle region, and a human placenta-specific 8 (PLAC8) domain (Pfam ID: PF04749) at the C-terminal region (Fig. 1). Recent phylogenetic analysis of MCA proteins showed that MCA is a land plant-specific protein with MCA functional (MCA^{fun}) and PLAC8 domains (Nishii et al. 2021). Thus, the analysis of *MpMCA* in *M. polymorpha* will provide evolutionary insights into the role of MCAs in the basic molecular mechanisms of growth and development in land plants.

MpMCA gene is expressed in the area where cell division activity is high in vegetative growth or sexual reproduction

Analysis of a public *M. polymorpha* transcriptome database (MBEX, <https://marchantia.info/mbex/>; Kawamura et al. 2022) indicated that *MpMCA* mRNA is ubiquitously expressed in all tissues, including the thallus, gemma cup, apical cells, antheridiophores, and archegoniophores (Supplementary Fig. S1). Next, the spatial pattern of *MpMCA* expression was examined using *MpMCA* promoter β -glucuronidase (*GUS*) or Citrine-NLS fusion reporter gene constructs (*proMpMCA:GUS* or *proMpMCA:Citrine-NLS*, respectively). When *proMpMCA:GUS* lines were cultured under continuous white light conditions, strong *GUS* staining was detected in the notch region of

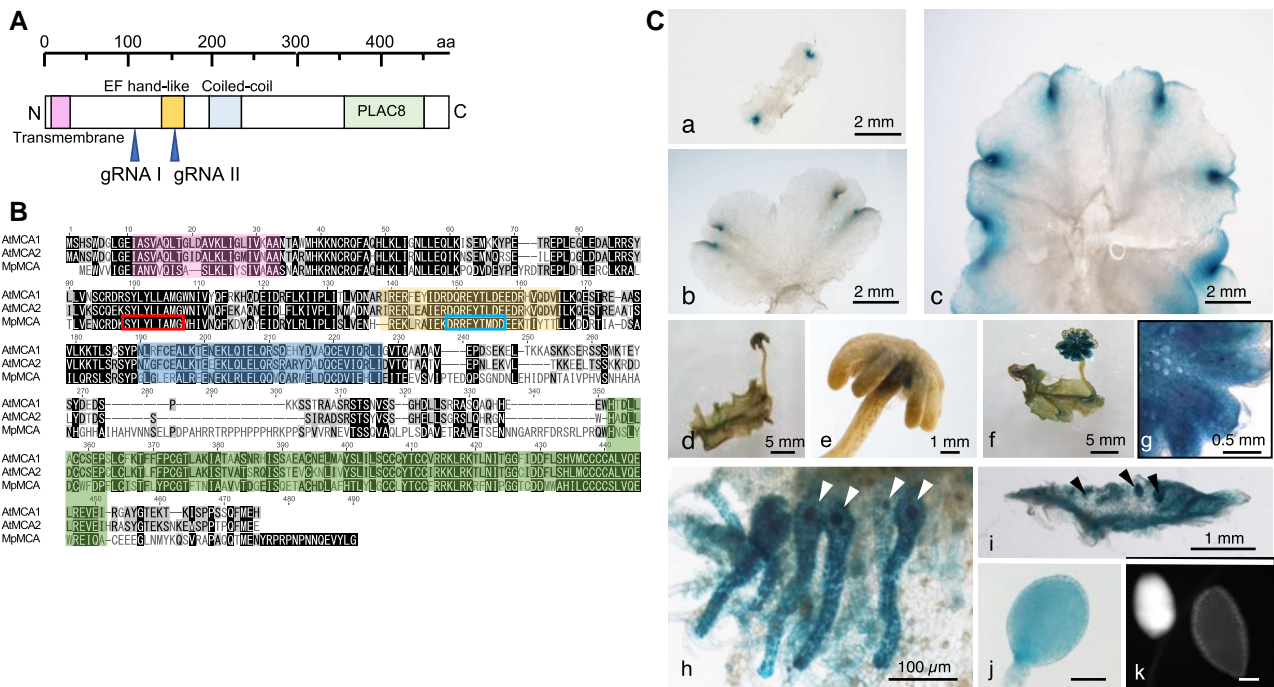


Figure 1. Domain structure of MpmCA protein and expression of MpmCA. **A)** Schematics of MpmCA protein. A ruler indicates the amino acid (aa) length. A transmembrane (pink), EF-hand like (yellow), a coiled-coil (sky blue), and PLAC8 (green) domains are indicated as each colored rectangle. The target position for two gRNAs is indicated by blue arrowheads. **B)** Sequence alignment of MpmCA, AtMCA1, and AtMCA2. Identical and conservative amino acid residues are shaded in black and grey, respectively. A transmembrane, EF-hand like, a coiled-coil, and PLAC8 domains are shaded in pink, yellow, sky blue, and green, respectively. Red box and blue box indicate the target position for gRNAI and gRNAII, respectively. **C)** *proMpmCA::GUS* transgenic lines stained by X-Gluc solution (a–j) and *proMpmCA::Citrine-NLS* line (k). (a–c) Thallus grown for 7 (a), 14 (b), and 21 d (c) under a white light condition. When female and male thalli were irradiated with FR, archegoniophore (d) and antheridiophore (f), respectively, were emerged at the thallus edge. Strong GUS staining was detected in the archegonial (e) and antheridial (f) disks. Cross sections of the disks show archegonia (h) and antheridia (i). In h and i, egg cells and antheridia are indicated by white and black arrow heads, respectively. Strong GUS staining or Citrine fluorescence were observed in the antheridia dissected from the antheridial disks of *proMpmCA::GUS* (j) or *proMpmCA::Citrine-NLS* (k), respectively. Similar results were reproducibly observed. Scale bars in j and k are 100 μ m.

the young thallus (Fig. 1C(a)), which was confined to this area even after branching of the thallus (Fig. 1C(b)), and slightly expanded to the wing region after 21 d (Fig. 1C(c)). When archegoniophore or antheridiophore formation was induced by a 1 mo FR irradiation, prominent GUS activity was observed in the disks, but not stalks, of both archegoniophores (Fig. 1, C(d) and C(e)) and antheridiophores (Fig. 1, C(f) and C(g)). In archegonia, GUS activity was prominent in the egg cells and was also detected in the cells surrounding the egg cells and neck cells (Fig. 1C(h)). GUS activity was detected prominently in antheridia in the cross-sections of the antheridiophore (Fig. 1C(i)) and was observed both in the spermatid and jacket cells (Fig. 1C(j)). In addition, when antheridia were observed in *proMpmCA::Citrine-NLS* line, strong promoter activity was observed in the spermatid and jacket cells of the young antheridia (left panel in Fig. 1C(k)). However, the expression was quite low in the mature antheridia, particularly in the inner region where mature sperm cells resided (right panel in Fig. 1C(k)). These results indicated that MpmCA probably functions in areas with high cell division activity in the apical notch region and reproductive organs (i.e. archegonia and antheridia).

MpmCA regulates cytoplasmic Ca^{2+} concentration in both vegetative growth and sexual reproduction

To examine whether MpmCA was involved in the regulation of $[Ca^{2+}]_{cyt}$, we generated transgenic plants expressing the Ca^{2+} sensor

protein yellow cameleon 3.60 (YC3.60) (Nagai et al. 2004). YC3.60 is a chimeric protein consisting of cyan fluorescent protein (CFP), calmodulin (CaM), a glycolylglycine linker, the CaM-binding domain of myosin light-chain kinase (M13), and the circularly permuted Venus protein (cpVenus). When the CaM domain binds Ca^{2+} , the domain associates with the M13 peptide, leading to an increase in Förster resonance energy transfer (FRET) between CFP and cpVenus, resulting in increased emission from the FRET acceptor, cpVenus (Fig. 2A). This technique is amenable to emission rationing, which is more quantitative than single-wavelength monitoring and is independent of the concentration of the sensor (Miyawaki et al. 2013; Grenzi et al. 2021; Miyata et al. 2023). The wild-type transgenic lines expressing YC3.60 under the control of the MpmCA promoter (*proMpmCA::YC3.60*) were generated to compare $[Ca^{2+}]_{cyt}$ at the MpmCA expression sites, such as notch region and gametangia, between wild type and *Mpmca*. The *proMpmCA::YC3.60* line was further manipulated using CRISPR/Cas9 technology to generate two independent *Mpmca* mutants (*Mpmca1-1^{ge}(F)*, *Mpmca1-2^{ge}(F)*, *Mpmca2-1^{ge}(F)*, and *Mpmca2-2^{ge}(F)*) (Supplementary Fig. S2). In the thalli, strong CFP and FRET (cpVenus) signals were observed at the apical notch region in all YC3.60 expressing lines (Fig. 2B), consistent with the MpmCA promoter activity visualized in the *proMpmCA::GUS* line (Fig. 1, C and a). CFP and FRET images of 3-d-old gemmalings were captured to compare the $[Ca^{2+}]_{cyt}$ of the wild type, *Mpmca* mutants (*Mpmca*) and complemented lines (*MpmCAcomp*). The intensities of CFP and FRET in the region of interest (ROI) (shown using white circles in Fig. 2B) were measured, and the ratio (FRET/CFP) reflecting $[Ca^{2+}]_{cyt}$

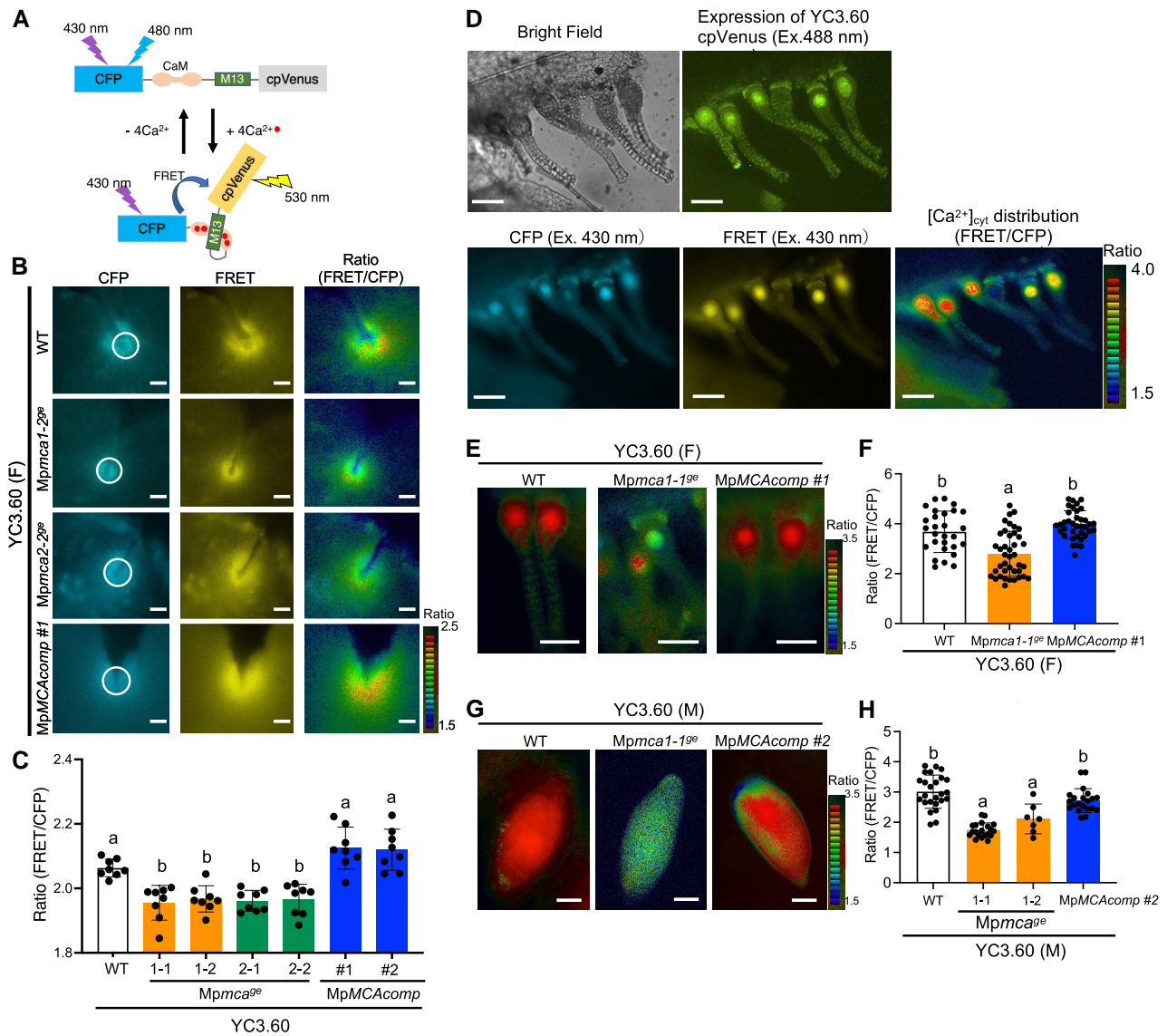


Figure 2. Distribution of $[\text{Ca}^{2+}]_{\text{cyt}}$ in gemmalings and gametangia of wild type, *Mpmca* mutant and complementary lines expressing *proMpMCA:YC3.60*.

A) Schematic representation of Förster resonance energy transfer (FRET)-based Ca^{2+} sensor, yellow cameleon 3.60 (YC3.60). Calmodulin (CaM) and the M13 peptide are bracketed by a FRET pair, CFP, and cpVenus. Calcium binding to calmodulin increases emission from the FRET acceptor. **B**) CFP and FRET images excited with 430 nm and ratio (FRET/CFP) image of wild type, two alleles *Mpmca* mutant, and *MpMCAcomp* in 3-d-old gemmalings. Scale bars = 50 μm . **C**) Ratio at the notch region of wild type, *Mpmca*, and *MpMCAcomp*. The intensity of the region of interest (ROI) (white circles) of CFP and FRET images was measured and the ratio (FRET/CFP) was calculated, respectively. Letters represent significant difference by one-way ANOVA and Tukey's multiple comparison test ($P < 0.001$). The data were expressed as mean \pm SD. ($n = 8$). **D**) Bright-field, cpVenus image excited with 488 nm light, CFP and FRET images excited with 430 nm and ratio image of wild-type archegonia expressing *proMpMCA:YC3.60*. Scale bars = 100 μm . **E–H**) Ratio images of wild-type, *Mpmca*, and *MpMCAcomp* and quantitative analysis of ratio in egg cells **E** and antheridia **G**. Letters indicate significant difference by one-way ANOVA and Tukey's multiple comparison test ($P < 0.001$). The data were expressed as mean \pm SD. (**F**, $n = 28\sim 40$; **H**, $n = 7\sim 25$) Scale bars = 100 μm .

was calculated (Fig. 2C). The ratio in the mutant was significantly lower than those in the wild-type or *MpMCAcomp* plants, suggesting a lower $[\text{Ca}^{2+}]_{\text{cyt}}$ in the mutant (Fig. 2C).

We examined $[\text{Ca}^{2+}]_{\text{cyt}}$ in the female or male gametangia of *proMpMCA:YC3.60*-expressing plants (*MpMCA:YC3.60*) to examine the regulation of $[\text{Ca}^{2+}]_{\text{cyt}}$ by MpMCA in the reproductive organs. A slice of an archegoniophore was cut off in females to examine $[\text{Ca}^{2+}]_{\text{cyt}}$ in archegonia. When cpVenus images excited with 488 nm light were observed to check YC3.60 expression in the archegonia, the expression of YC3.60 was detectable in all cell types, including the egg, neck, and egg cell-surrounding cells (Fig. 2D). By analyzing the ratio images (FRET/CFP) of wild-type plants, it was

evident that $[\text{Ca}^{2+}]_{\text{cyt}}$ in egg cells were much higher than that in neck cells and egg cell-surrounding cells (Fig. 2D). In contrast, $[\text{Ca}^{2+}]_{\text{cyt}}$ in the egg cells of *Mpmca* was significantly lower than that in the wild type and complemented lines (*MpMCAcomp*) (Fig. 2, E and F). These results indicated that MpMCA is involved in regulating $[\text{Ca}^{2+}]_{\text{cyt}}$ in egg cells.

Furthermore, we examined whether MpMCA was involved in regulating $[\text{Ca}^{2+}]_{\text{cyt}}$ in antheridia by comparing the YC3.60 ratios in *Mpmca* and *MpMCAcomp* plants harboring the MpMCA:YC3.60 construct. Since the receptacle size in *Mpmca* plants was small and the antheridia was immature, we isolated immature antheridia from the receptacles at Stage 3 (Higo et al. 2016). The same procedure

was repeated for wild-type and *MpMCAcomp* genetic backgrounds. Thus, we compared the ratios (FRET/CFP) in the antheridia of the different genotypes, revealing that the $[Ca^{2+}]_{cyt}$ in *Mpmca* antheridia was lower than that in the wild-type and *MpMCAcomp* lines (Fig. 2, G and H). These results indicate that MpMCA is involved in regulating $[Ca^{2+}]_{cyt}$ during antheridium development and possibly mediates cell division during spermiogenesis via Ca^{2+} signaling.

Collectively, MpMCA regulates $[Ca^{2+}]_{cyt}$ in regions with high division activity, such as the apical notch in the thalli and developing sexual organs.

MpMCA regulates cytoplasmic Ca^{2+} concentration during gemma hydration to germination and in response to osmotic stress

We generated wild-type and *Mpmca* transgenic plants expressing YC3.60 under the control of the *MpEF* promoter (*proMpEF*:YC3.60), which is active in meristematic cells (Althoff et al. 2014; Tse et al. 2024) to examine whether MpMCA regulates $[Ca^{2+}]_{cyt}$ in the notch and in the area surrounding the notch. We then analyzed the $[Ca^{2+}]_{cyt}$ dynamics of dormant gemmae during hydration and germination every 5 min for 18 h. The ratio (FRET/CFP) at the notch area in the gemma of the wild type increased slightly during the observation period, but this increase was not detected in *Mpmca*. In particular, we compared the YC3.60 ratios of the wild-type and mutant plants 15 h after the start of the experiment, where the difference was significant (Figs. 3, A to C, Supplementary Videos S1 and S2). This result showed that the $[Ca^{2+}]_{cyt}$ in the area surrounding the notch in the gemma of the wild type was higher than that in *Mpmca*, suggesting that MpMCA is involved in the regulation of $[Ca^{2+}]_{cyt}$ during hydration and germination. Furthermore, a dot-like pattern of high $[Ca^{2+}]_{cyt}$ was observed in the central area of the wild-type gemmae but not in the *Mpmca* gemmae (Fig. 3, A and B). Rhizoid precursor cells, which are larger and paler than the surrounding epidermal cells in the bright field (BF) observation, were found in the central area of the gemma in the wild type (Proust et al. 2016). Comparison between BF and FRET images on the surface of gemmae at 1 h after hydration revealed overlaps of dot-like FRET signals with translucent rhizoid precursor cells (Fig. 3D), which allowed us to find that the number of rhizoid precursor cells was significantly lower in *Mpmca* gemmae than that in the wild type (Fig. 3, D and E). Furthermore, because *AtMCA1*, *NtMCAs*, and *OsMCA* are implicated in the mechanical stress signaling (Nakagawa et al. 2007; Kurusu et al. 2012a, 2012b), hyperosmotic stress by exogenous application of mannitol was given to 8-d-old gemmaling highly expressing *proMpEF*:YC3.60. After the addition of mannitol, $[Ca^{2+}]_{cyt}$ in the notch surrounding area was elevated to about 1.5 times than the basal level before addition in the wild type (Fig. 4A; Supplementary Video S3), while $[Ca^{2+}]_{cyt}$ was elevated to approximately 1.2 times than the basal level in *Mpmca* (Fig. 4B; Supplementary Video S4).

Overall, these results suggested that MpMCA is required for the regulation of $[Ca^{2+}]_{cyt}$ under both mechanically non-stressed and stressed conditions.

MpMCA is essential for the normal growth and development of the vegetative tissue

We generated *Mpmca* by gene editing with CRISPR/Cas9 using wild-type Tak-2×Tak-1 spores to further characterize the function of MpMCA (Fig. 5, Supplementary Fig. S2). When plants were cultured from a gemma for 1 mo under continuous white light conditions on half-strength Gamborg's B5 agar medium with sucrose, the thalli of the wild-type accessions (Tak-2 for females [WT(F)] and Tak-1 for

males [WT(M)]) had several branches with multiple gemma cups (Fig. 5, A(a) and A(e)). The thalli of WT(F) were curled (Fig. 5A(a)), whereas those of WT(M) were flattened (Fig. 5A(e)). However, the thalli of the *Mpmca* lines (*Mpmca-1^{ge}(F)* and *Mpmca-2^{ge}(M)*) (Fig. 5A(b) for female lines, and f for male lines) exhibited a smaller surface area, decreased branching, a smaller number of gemma cups, and lower fresh weight than the wild type (Fig. 5, A(b), A(f), B and C). Furthermore, mutant thalli were curled irrespective of sex (Fig. 5, A(b) and A(f)). These mutant phenotypes were complemented by introducing MpMCA cDNA containing CRISPR/Cas9-resistant synonymous mutations (*MpMCAcomp*) (Fig. 5, A(c) and A(g)). These results indicated that MpMCA is required for vegetative tissues to grow and develop.

We performed a thymidine analog EdU incorporation assay to visualize S-phase progression and further characterize the growth of vegetative tissue in *Mpmca*. Strong EdU incorporation was confined to the apical notch region containing meristematic cells in 3-d-old gemmae of the wild type and complement lines (Fig. 5D). EdU incorporation was also observed in the apical notch region in *Mpmca* but was significantly decreased and sparse compared with that in the wild-type and complemented lines (Fig. 5, D and E). Bifurcation of both the notch and EdU incorporation areas (arrowheads in Fig. 5D), indicative of branching of thalli, was observed in the wild type and the complemented line after 7 d, while such bifurcation was rarely observed in *Mpmca* at this stage (Fig. 5, D and E), consistent with the reduced branching in *Mpmca* (Fig. 5, A(b) and A(f)). Importantly, the EdU incorporation area (Fig. 5D) overlapped with strong MpMCA expression sites visualized in the *proMpMCA*:Citrine-NLS line (Fig. 5F). In addition, the expression of *MpCYCD;1*, a gene encoding a D-type cyclin that serves as a cell division marker in *M. polymorpha* (Ishida et al. 2022), was significantly lower in *Mpmca* than in the wild type (Fig. 5G). These results indicated that the growth defect in *Mpmca* was due to the inhibition of cell proliferation during vegetative growth. Furthermore, these results were supported by the analysis of the two allelic *Mpmca* mutants in the *proMpMCA*:YC3.60 transgenic background. These mutant gemmalings exhibited severe growth defects and a coordinated decrease in the gemma cup with a decrease in *MpCYCD;1* gene expression on Day 21 (Supplementary Fig. S3, A to E).

When we observed the apical notch of the wild-type and *Mpmca* dormant gemmae in the cup with transmission electron microscopy (TEM), many lipid body-like structures were observed in the notch region of the gemma of the wild type (Fig. 5H(a)), while the structure was rarely observed in that area in the *Mpmca* (Fig. 5H(b)) and immature gemmae connected to the stalk (Fig. 5, H(c) and H(d)). These observations suggested that lipid storage associated with dormancy is arrested in *Mpmca*. In addition, the primary cell wall and middle lamella were observed in the wild-type gemma (inset of Fig. 5H(a)), but it was difficult to distinguish the primary wall from the middle lamella in *Mpmca* (inset of Fig. 5H(b)). This suggested that the cell wall composition of *Mpmca* was different from that of the wild type.

To know where MpMCA functions in the apical notch cells, we generated *Mpmca* mutant producing a mNeonGreen fusion protein to the C-terminus of the full-length MpMCA (*MpMCA*_mNeonGreen) by introducing *MpMCAproMpMCAcomp_mNeonGreen*. The expression of MpMCA-mNeonGreen complemented *Mpmca* mutant phenotypes (Supplementary Fig. S4). Fluorescence of MpMCA-mNeonGreen was present in the plasma membrane of apical notch cells (Fig. 5, I(a) and I(c)). The fluorescence was obviously detected on the cell membrane associated with the neighboring cells, but not on the outermost cell side (Fig. 5I(a)), suggesting the polarized localization of MpMCA.

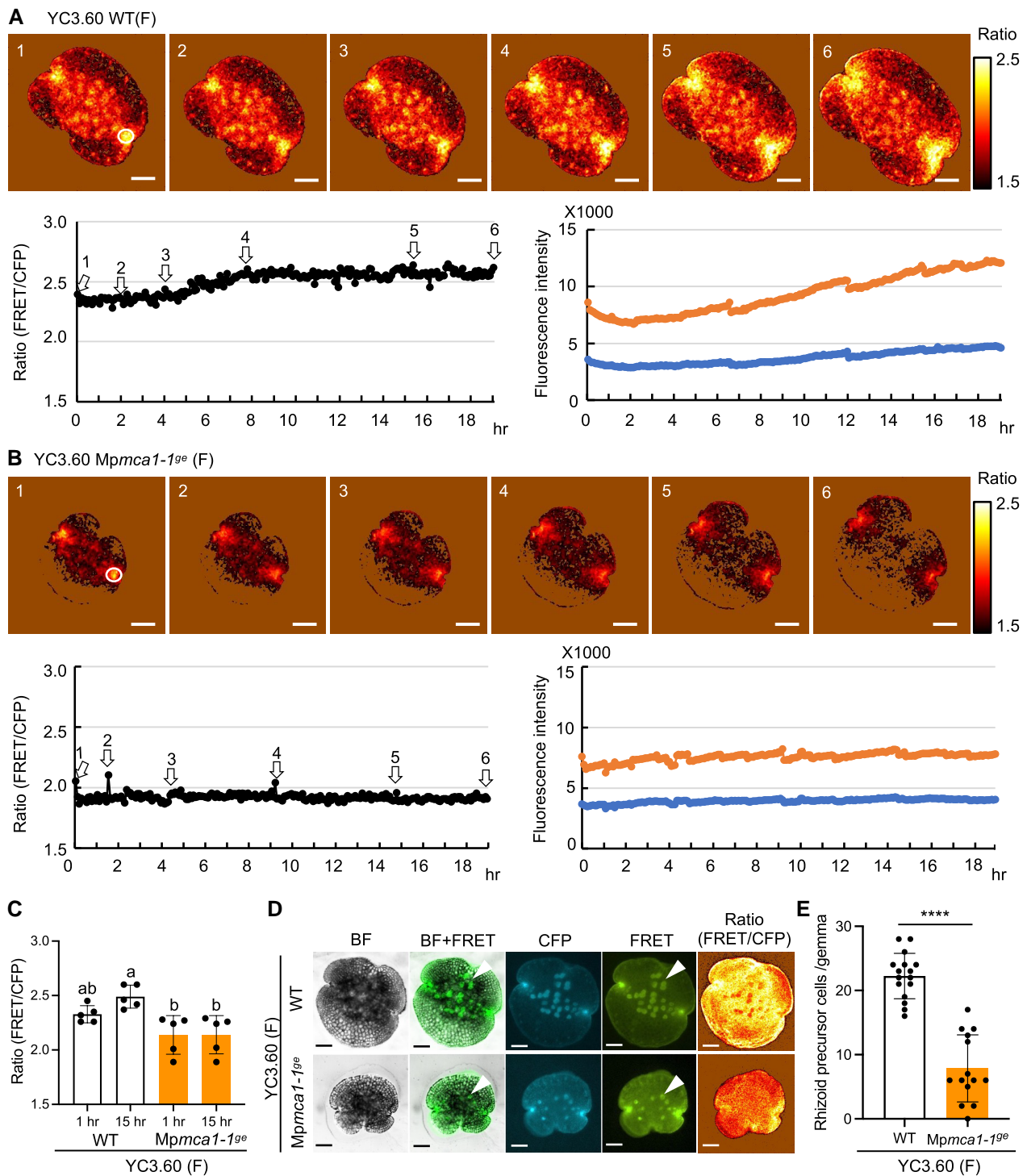


Figure 3. $[Ca^{2+}]_{cyt}$ change and the rhizoid precursor cells of wild-type and *Mpmca* mutants expressing *proEF::YC3.60*. **A,B**) $[Ca^{2+}]_{cyt}$ changes during just after gemma hydration to germination. The upper images are the ratio images (FRET/CFP) in wild type (A) and *Mpmca* (B) lines, respectively. The left panel shows ratio changes of the ROI (a white circle in A1 or B1) at a notch region. The right panel shows the intensity of CFP and FRET of the ROI (a white circle in A1 or B1). Numbers in the left panel correspond to each image number of A or B. **C**) Comparison between wild-type and *Mpmca* ratios at 1 h or 15 h after hydration, respectively ($n = 5$). Letters indicate significant difference by ordinary one-way ANOVA and Tukey's multiple comparison test ($P < 0.01$). **D,E**) BF, FRET, CFP, and ratio images of the surface of gemmae at 1 h after hydration (**D**) and the number of the rhizoid precursor cells (**E**). Arrowheads show the rhizoid precursor cells. Asterisks indicate significant difference compared with *Mpmca* by Student's two-tailed unpaired t-test (****; $P < 0.0001$). Scales bars = 100 μ m.

Collectively, these results indicated that MpMCA regulates vegetative growth and development via the maintenance of cell proliferation on the plasma membrane in the apical notch regions.

MpMCA is necessary for sexual reproduction

Sexual reproduction in *M. polymorpha* is induced by supplementation with FR irradiation under long-day conditions. Wild-type, *Mpmca*, and *MpMCAcomp* lines were grown under continuous

white light for 7 d and then irradiated with supplemental FR to induce gametangiophore formation to investigate the role of MpMCA in sexual reproduction (Fig. 6, A and B). In female lines, archegoniophore formation in the wild type began approximately 14 d after FR irradiation (Fig. 6, A(a) and C). However, in *Mpmca*, archegoniophore formation was significantly delayed, and the total number of archegoniophores was greatly decreased compared with that in the wild type (Fig. 6, A(b) and C). The defects in the timing and number of archegoniophore formations were complemented by the introduction of *MpMCAcomp* (Fig. 6, A(c) and C). In male lines, antheridiophore formation in the wild type was observed ca. 9 d after FR irradiation (Fig. 6, B(a) and D), which is earlier than archegoniophore formation in the wild-type females (Yamaoka et al. 2018). In *Mpmca*, the antheridiophore formation was minimally induced (Fig. 6, B(b) and D). In *MpMCAcomp* male lines, antheridiophore formation recovered but was delayed compared with that in wild-type males (Fig. 6, B(c) and D). These results indicated that MpMCA is required for sexual reproduction.

MpMCA is involved in the development of gametangia

Cross sections of the archegoniophores were observed using light microscopy (LM) and TEM to compare the morphology of archegonia in *Mpmca* with that of the wild type. The egg cells in the wild type were round, the surface was smooth, and the cells surrounding the egg cells were well organized (Fig. 6, A(e) and A(f)). However, egg cells and surrounding cells were distorted in *Mpmca* (Fig. 6, A(g) and A(h)), indicating that archegonial development was impaired in *Mpmca*. A wild-type sperm droplet was applied to archegoniophores in female lines of wild type, *Mpmca*, and *MpMCAcomp* to examine whether successful fertilization was performed in the egg cells of *Mpmca*. Although sporangia formation was observed in wild type (Fig. 6A(i)) and *MpMCAcomp* (Fig. 6A(k)) plants, sporangia were rarely formed in *Mpmca* (Fig. 6A(j)), indicating that MpMCA was required for successful fertilization.

During antheridiophore development in the wild type, the antheridial receptacle showed a shallow cup-like structure with a bump at the center (Fig. 6B(e)) (Higo et al. 2016). Antheridiophores were scarcely formed in *Mpmca* (Fig. 6B(b)), and even if they did form, their development was immature (Fig. 6B(f)). When water was applied to the top of the mature antheridial disks, sperm were released in the wild type (Fig. 6B(i)) and *MpMCAcomp* (Fig. 6B(j)), but not in *Mpmca*. When sperm nuclei were observed with DAPI staining, the shape of the sperm nuclei did not differ between the wild type (Fig. 6B(i)) and *MpMCAcomp* (Fig. 6B(j)). We collected antheridiophores from the wild type (at Stages 1 to 4) and from *Mpmca* and observed them using LM and TEM to examine whether the formation of antheridia was arrested in *Mpmca*. At Stage 3, immature antheridia were observed in the wild-type lines (Fig. 6B(l); LM). Higher magnification images showed that spermatogenous cells (SC) repeatedly divided to form many uniform SC cells (Fig. 6B(m); LM). In contrast, the antheridiophores of *Mpmca* contained many antheridia (Fig. 6B(n); LM), but the cell size and shape of SC were disorganized, suggesting that cell division of SC was impaired in *Mpmca* (Fig. 6B(o); LM). When we further compared the structure of the wild type with that of *Mpmca* using TEM, jacket cells and SC were relatively uniform and surrounded by a cell wall of nearly uniform thickness in the wild type (Fig. 6B(p)), whereas the shapes of both jacket cells and SC were distorted in *Mpmca* (Fig. 6B(r)). In addition, SC in the wild type contained normal nuclei, small vacuoles, and plastids (Fig. 6B(q)), whereas SC in *Mpmca* was filled with granular structures, suggesting that cell division was impaired

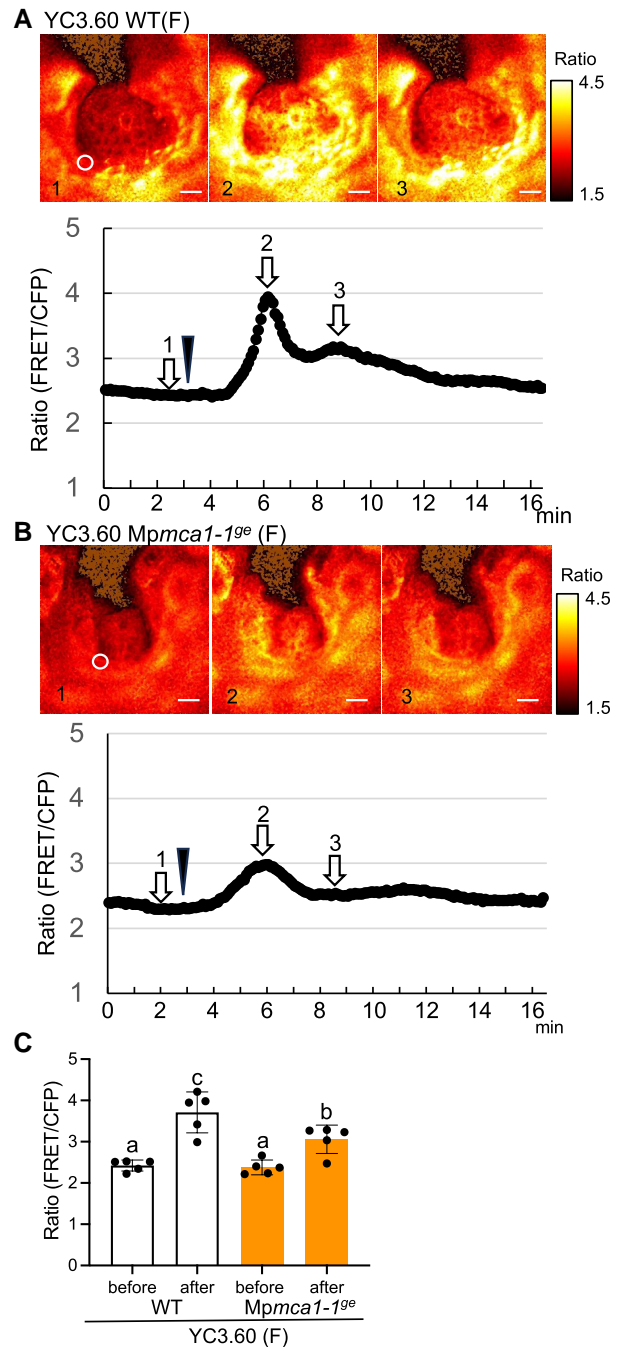


Figure 4. $[Ca^{2+}]_{cyt}$ change induced by osmotic stress at the notch of wild-type and *Mpmca* mutants expressing *proEF::YC3.60*. **A,B** $[Ca^{2+}]_{cyt}$ changes before and after the addition of mannitol solution. 8-d-old gemmaling was mounted on the glass-bottomed dish and covered with a small amount of 1/2 Gamborg's medium. For giving osmotic stress, 1/2 Gamborg's medium containing 0.4 M mannitol solution was added to the dish to a final concentration of 200 mM. Arrowheads show timing when mannitol solution was added. The upper images are the ratio images (FRET/CFP) in wild-type (A) and *Mpmca* (B) lines, respectively. The under panel shows ratio changes of the ROI (a white circle in A1 or B1) at a notch region. The data were collected every 6 s for 18 min. Scales bars = 100 μ m. **C** Comparison between wild-type and *Mpmca* ratios before or the maximum value after the addition of mannitol solution, respectively. Letters indicate significant difference by ordinary one-way ANOVA and Tukey's multiple comparison test ($P < 0.01$). The data were expressed as mean \pm SD ($n = 5$).

and cell death occurred in *Mpmca* (Fig. 6B(s)). These results indicated that MpMCA is essential for coordinated cell division during spermiogenesis.

MpMCA functions in very early stage of gametangiophore development

The early developmental stages of antheridiophore formation were examined using LM and TEM to further examine the role of *Mpmca* in gametangiophore formation (Fig. 6, E to G). The gametangiophores started to emerge 8 or 9 d after FR irradiation in the wild-type male line (Fig. 6D). Thus, we fixed the thalli of wild-type and *Mpmca* days after FR irradiation and observed the vertical sections, which are perpendicular to the midrib at the notch, using LM and TEM (Fig. 6F). A part of the immature tissue of the gametangiophore was observed as a cell clump only on one side of the bifurcated notches in the wild type using LM (Fig. 6, F(a) and F(c)). However, the bifurcated notch was unclear, and cell clumps could not be observed in *Mpmca* (Fig. 6, F(b) and F(d)). Some undifferentiated and round cells were observed at the surface of the cell clump in the wild type using TEM, but not in the notch region of *Mpmca* (Fig. 6, F(e) and F(f)). Furthermore, 7 d after FR irradiation, very small antheridiophores with early stage antheridia were observed on the ventral side of the wild-type thalli using field emission scanning electron microscopy (FE-SEM) (Toyooka et al. 2023). Therefore, these LM, TEM, and FE-SEM observations show that MpMCA functions in the very early stages of gametangiophore development.

Function of MpMCA in growth and development in *M. polymorpha* is conserved in AtMCA1

We examined whether MpMCA could complement lethality in the *S. cerevisiae* *mid1 cch1* double mutant, similar to seed plant MCAs. Compared with the empty vector control cells, FLAG-tagged AtMCA1 or AtMCA2 partially rescued this lethality. FLAG-tagged or untagged MpMCA weakly complemented lethality at a level comparable to AtMCA2 expressing cells (Supplementary Fig. S5A). However, unlike AtMCA1 and AtMCA2, MpMCA exhibited no detectable complementary activity for Ca^{2+} uptake defects in the *mid1 cch1* double mutant (Supplementary Fig. S5B). MpMCA or AtMCA1 was introduced into cells of the low-affinity Ca^{2+} -uptake-deficient yeast mutant strain K667 to determine whether MpMCA has Ca^{2+} transport activity in yeast cells. This strain is a triple mutant strain deficient in the vacuolar ATPase PMC1, vacuolar $\text{H}^+/\text{Ca}^{2+}$ exchanger VCX1, and calcineurin regulatory subunit CNB1, and shows Ca^{2+} -uptake deficiency and low Ca^{2+} tolerance (Cunningham and Fink 1996; Pittman and Hirschi 2001). Cells of the transgenic K667 strain expressing MpMCA or AtMCA1 grew well on a plate containing an ordinary concentration of CaCl_2 (1 mM), similar to those containing the empty vector. However, they were slightly sensitive to 50 and 100 mM Ca^{2+} , suggesting that MpMCA and AtMCA1 are involved in regulating Ca^{2+} homeostasis, at least in the K667 strain (Supplementary Fig. S6).

The MpMCA promoter-driven *A. thaliana* MCA1 gene construct (*proMpMCA:AtMCA1*) was introduced into *Mpmca* to test whether the function of MpMCA is conserved during land plant evolution. Growth defects in gemmaling and thalli in the *Mpmca* lines were complemented by the introduction of AtMCA1 (Fig. 5, A(d) and A(h)), indicating that AtMCA1 retains the ability to regulate growth and development in *M. polymorpha*.

When grown under continuous white-light conditions for 7 d and then irradiated with supplemental FR (Fig. 6, A to C, and D), the defect in archegoniophore formation of *Mpmca* was complemented strongly by introducing AtMCA1 into female lines (Fig. 6, A(d) and C); however, the complementation was less in AtMCA1 male lines than *MpMCAcomp* male lines (Fig. 6, B(d) and D).

When the egg cell of AtMCA1 was crossed with wild-type sperm, sporangia formation was observed, indicating that the egg cell of AtMCA1 was successfully fertilized (Fig. 6A(l)). In male lines, growth inhibition of antheridia in *Mpmca* was rescued by AtMCA1 (Fig. 6B(d)), and the shape of the sperm nuclei in AtMCA1 lines was not different from that of the wild type (Fig. 6A(k)). These results suggested that AtMCA1 complements most defects in the growth and development of thalli, gametangiophores, and gametangia in *Mpmca*.

Both MpMCA and AtMCA had partial MCA in yeast, but only AtMCA1 had Ca^{2+} uptake activity (Supplementary Fig. S5B). In contrast, AtMCA1 regulated the growth and development of the thalli, gametangiophores, and gametangia in *M. polymorpha*.

Discussion

MCA is a land plant-specific protein associated with mechanosensitive channel activity that permeates Ca^{2+} ions (Nishii et al. 2021) and has been characterized as a pivotal molecule that regulates plant growth and development (Kurusu et al. 2013; Rosa et al. 2017). However, how MCA regulates plant growth and development remains unclear. Our detailed analysis of the liverwort *M. polymorpha* MCA ortholog MpMCA sheds light on the role of MCA in growth and development and the possible link between Ca^{2+} signaling and cell proliferation in land plants.

MpMCA is essential for regulating $[\text{Ca}^{2+}]_{\text{cyt}}$ at the actively dividing cells

AtMCA1 and/or AtMCA2 are involved in $[\text{Ca}^{2+}]_{\text{cyt}}$ increase induced by various exogenous stresses, including hypergravity, cold, and osmotic stresses (Nakagawa et al. 2007; Yamanaka et al. 2010; Mori et al. 2018; Hattori et al. 2020; Nakano et al. 2021; Okamoto et al. 2021; Nakano et al. 2022). NtMCA1/2 and OsMCA can regulate a $[\text{Ca}^{2+}]_{\text{cyt}}$ increase induced by hypoosmotic stress in yeast cells or cultured cells of tobacco and rice (Kurusu et al. 2012a, 2012b). However, it remains unclear whether MCAs are involved in regulating $[\text{Ca}^{2+}]_{\text{cyt}}$ in cell proliferation and differentiation during normal growth and development under conditions free of external stress. We found that MpMCA is a plasma membrane protein (Fig. 5) and involved in the external osmotic stress (Fig. 4). In addition, we examined the potential involvement of MpMCA in regulating $[\text{Ca}^{2+}]_{\text{cyt}}$ during normal growth and development of *M. polymorpha* plants to clarify this. Cell proliferation activity decreased at the apical notch in the *Mpmca* mutant (Fig. 4), concomitant with lower $[\text{Ca}^{2+}]_{\text{cyt}}$ at the apical notch in the mutant than in the wild type under external stress-free conditions (Fig. 2, B and C) and lower $[\text{Ca}^{2+}]_{\text{cyt}}$ changes during hydration to germination (Fig. 3). Thus, our findings indicated that MpMCA regulates $[\text{Ca}^{2+}]_{\text{cyt}}$ at the plasma membrane of the apical notch to maintain cell proliferation.

Furthermore, the imaging of $[\text{Ca}^{2+}]_{\text{cyt}}$ dynamics in pollen tube growth and the related Ca^{2+} transporters have been studied extensively (Schjøtt et al. 2004; Lucca and León 2012; Chen et al. 2015); however, there are few studies on the role of $[\text{Ca}^{2+}]_{\text{cyt}}$ in pollen development and megagametogenesis in angiosperms. In this study, Ca^{2+} imaging in *M. polymorpha* revealed high $[\text{Ca}^{2+}]_{\text{cyt}}$ in the archegonium, particularly in egg cells, in female wild-type plants, and in the developing antheridium in male wild-type plants. However, $[\text{Ca}^{2+}]_{\text{cyt}}$ was significantly lower in the same tissues of *Mpmca* than in the wild type. Severe defects in gametophore formation and impaired fertility observed in the *Mpmca* mutant suggest that MpMCA is essential for regulating $[\text{Ca}^{2+}]_{\text{cyt}}$, leading to the development of reproductive tissues and fertilization. As both egg cell

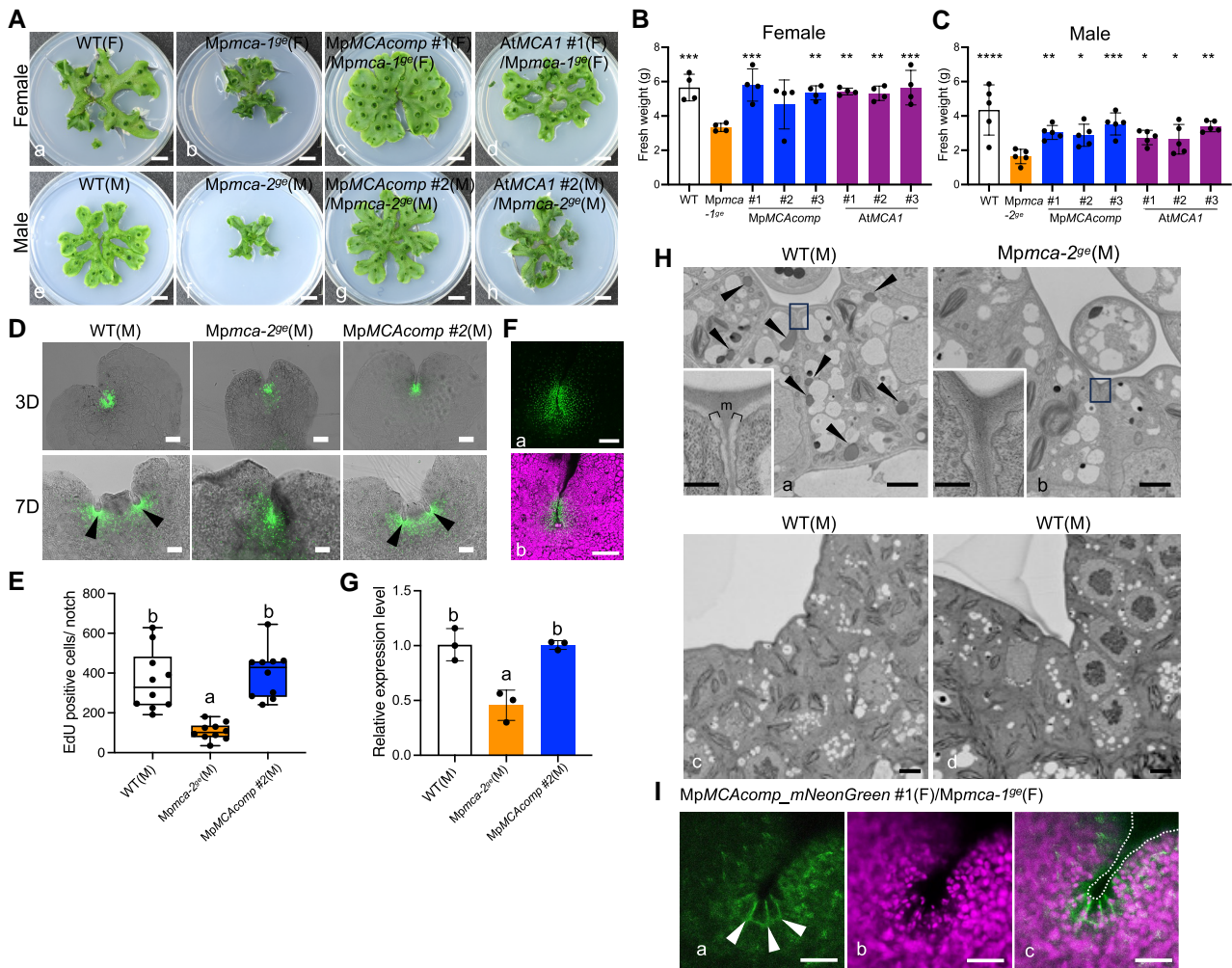


Figure 5. Phenotype in the vegetative growth of wild-type, *Mpmca*, and the complemented lines, *Mpmca* expressing *MpMCA* complement (*MpMCAcomp*) or *AtMCA1* (*AtMCA1*). **A**) Growth and development of thalli. 4-wk-old thallus female (a–d) and male (e, f) grown on 1/2 Gamborg’s medium containing 10% sugar under continuous white light. WT(F) and WT(M) are wild-type accessions, Tak-2 and Tak-1, respectively. Scale bars = 1 cm. **B,C**) Fresh weight in 4-wk-old thallus of female or male lines (B, $n = 4$; C, $n = 5$). Asterisks indicate significant difference compared with *Mpmca* by Student’s two-tailed unpaired t-test (*; $P < 0.05$, **; $P < 0.01$, ****; $P < 0.0001$). Bars represent mean \pm SD. **D,E**) Analysis of cell proliferation in apical notch region of gemmalings in wild-type, *Mpmca*, and *MpMCAcomp* male lines. **D**) EdU incorporated cells (green) in 3-d-old (upper panels) and 7-d-old (lower panels) gemmalings after incorporation of EdU for 4 h. Arrowheads show the notch. Scale bars = 100 μ m. **E**) The number of EdU-incorporated cells per single notch in 3-d-old gemmalings ($n = 10$). Whiskers, maximum, and minimum values; box limits, upper, and lower quartiles; center line, median. **F**) *MpMCA*-expressed cells (green) visualized in *proMpmCA::Citrine-NLS* (a) in 3-d-old gemmalings. Magenta signal in (b) shows chlorophyll autofluorescence. Scale bars = 100 μ m. **G**) Relative expression level of *MpCYCD;1* determined by qRT-PCR of 3-d-old gemmalings ($n = 3$). Letters in (E) and (G) indicate significant difference compared with *Mpmca* by one-way ANOVA and Dunnett’s multiple comparison test ($P < 0.01$). Bars represent mean \pm SD. **H**) TEM image of the apical notch in wild-type (a, c, d) and *Mpmca* (b) dormant gemmae and wild-type developing gemmae (c, d) on the stalk in the cup. The stage of (c) is earlier than that of (d). Arrowheads show lipid bodies. Each inset shows a magnified image of a black square. Brackets in the inset show the primary wall. Middle lamella (m). Scale bars = 2 μ m. Scale bars in insets = 0.5 μ m. **I**) Localization of *MpMCAcomp_mNeonGreen* (arrowheads) in the plasma membrane of apical notch in gemmae of *Mpmca-1^{9e}*(F) expressing *proMpmCA::MpMCAcomp_mNeonGreen* (a). Magenta signal in (b) shows chlorophyll autofluorescence. (c) shows an overlapping image of (a) and (b). White dotted line in (c) shows the edge of apical notch. Scale bars = 20 μ m.

formation and spermiogenesis result from active cell proliferation and differentiation that can produce intercellular mechanical pressure, *MpMCA* may be involved in the Ca^{2+} signaling pathway induced by endogenous mechanical forces in both vegetative growth and sexual reproduction.

MpMCA regulates plant growth and development through the control of cell division and morphogenesis during both vegetative growth and sexual reproduction

The growth and development of dicot *mca* mutant plants, including *Arabidopsis* and *N. tabacum*, are mild under stress-free conditions,

and growth defects appear only under severe stress conditions (Nakagawa et al. 2007; Yamanaka et al. 2010; Kurusu et al. 2012b; Mori et al. 2018; Hattori et al. 2020; Okamoto et al. 2021). In contrast, in monocots, *mca* mutant plants, including *Oryza sativa* (*pad*, *dwarf*, and *multi-tillering1 [dmt1]* mutant) and *Zea mays* (*nod* mutant), exhibit prominent growth and developmental defects under stress-free conditions (Liu et al. 2015; Rosa et al. 2017; Liang et al. 2020). Similar to monocot *mca* mutant plants, *Mpmca* mutants showed severe growth and developmental defects even under external stress-free conditions, including slower growth and organ initiation during vegetative growth, impaired sexual reproduction, and malformation of gametophore organs and tissues. The only subtle

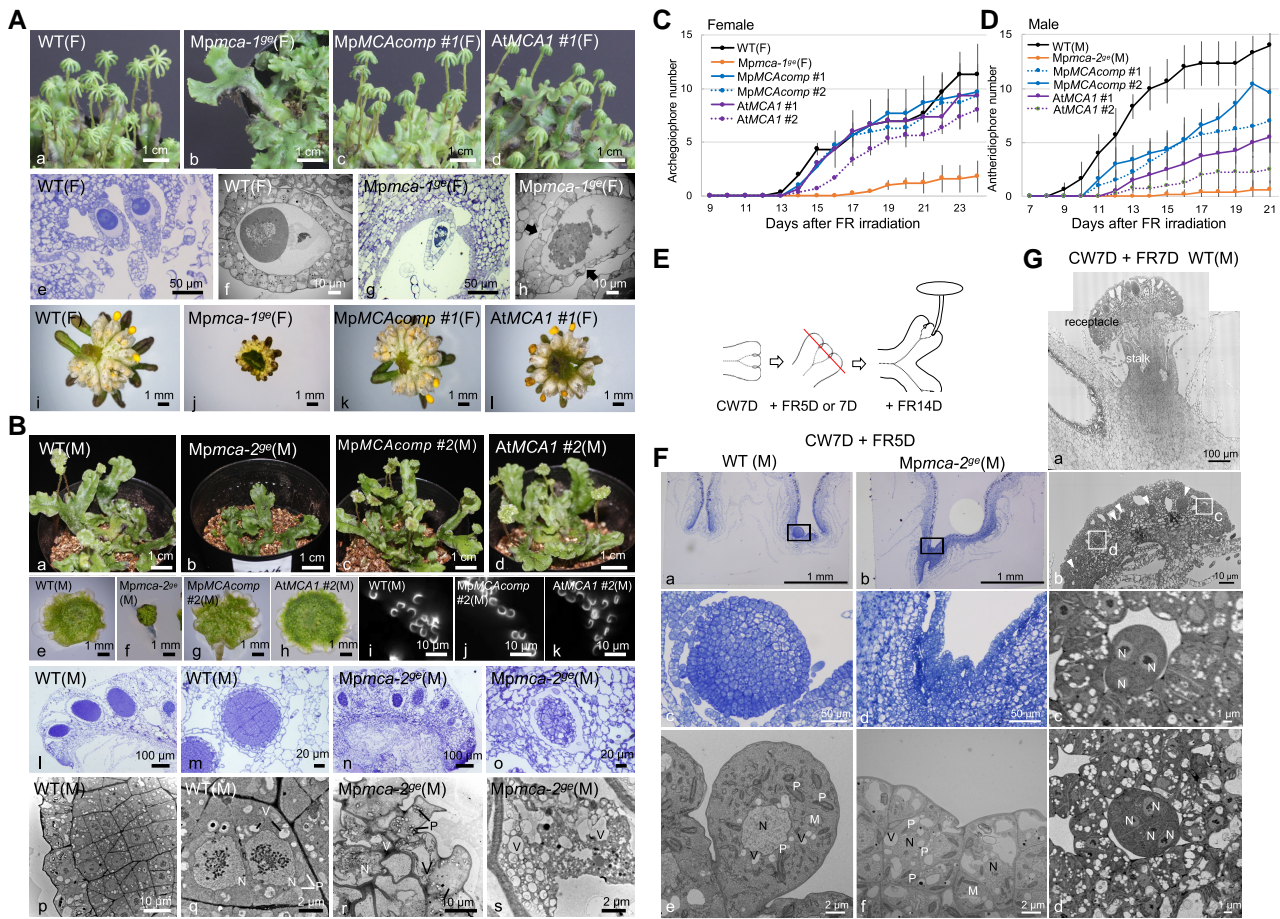


Figure 6. Phenotype in the reproductive phase of wild-type, *Mpmca*, and the complemented lines, *Mpmca* expressing *MpMCAcomp* or *AtMCA1* (*AtMCA1*). **A**) Archegoniophore formation and morphological analysis in female plants at 1 mo after FR irradiation (a–d), archegoniophore formation (e–h), wild-type (e, f) and *Mpmca* (g, h) archegonia observed with LM (e, g), and TEM (f, h). In *Mpmca*, distortion in the egg cell and in the cells surrounding egg cell (arrows in h) was observed. (i–l). Sporophyte formation when crossed with wild-type sperms. **B**) Antheridiophore formation (a–d) and morphological analysis in male plants at 1 mo after FR irradiation. Antheridiophore (e–h) and sperm cells stained with DAPI (i–k). Cross section of antheridia of wild type (l, m, p, and q) and *Mpmca* (n, o, r, and s) observed with LM (l–o) and TEM (p–s). Nucleus (N), vacuole (V), and plastids (P). **C, D**) Time-course analysis of archegonia and antheridiophore formation after FR irradiation. Bars represent mean \pm SD from five independent experiments. **E**) Scheme of antheridiophore formation and cutting position (red line) for LM and TEM observation. **F**) Vertical cross section to midrib in notch region of thallus at 5 d after FR irradiation. Tissue and cell structure were observed with LM (a–d) and TEM (e, f). Cell clump (arrows) observed at one side of notch region of wild type. Square regions (c, d) in b were magnified in c and d, respectively. **G**) Cross section of immature wild-type antheridiophore at 7 d after FR irradiation observed with FE-SEM. (a) A panorama (composite) image of immature antheridia (arrowheads) consisting of 35 images. (b) A higher magnification of immature antheridia. Arrowheads show immature antheridium. Square region in b was magnified in c and d, respectively. Plastids (P), nucleus (N), and mitochondria (M).

defects in dicot *mca* mutant plants suggest that dicots might have evolved an additional mechanical Ca^{2+} channel system to mediate growth and development. For example, *Arabidopsis* has many Ca^{2+} -permeable channel proteins, which are believed to function as mechanical Ca^{2+} -permeable channels and potentially play a crucial role in various stress response (Guichard et al. 2022). *M. polymorpha* has a much smaller set of calcium-permeable channel genes, five CNGC, one *GLR*, four *OSCA*, one *PIEZO*, and three *TPC* genes (Marchetti et al. 2021; Watanabe et al. 2024; Wu et al. 2022; Radin et al. 2021; Hashimoto et al. 2022). Thus, the contribution of *MpMCA* to growth and development could be great in *M. polymorpha*.

Severe defects in *Mpmca* mutants were accompanied by morphological changes in the cell wall structure (Fig. 5, H(a) and H(b)) and cell wall deformation (Fig. 6, A(l), B(r), and B(s)), suggesting a change in the cell wall composition in *Mpmca*. However, the report that *AtMCA1* is involved in the perception of cell wall damage induced by an inhibitor of cellulose biosynthesis or a cell wall degradation enzyme in *Arabidopsis* (Engelsdorf et al. 2018) supports this.

Plants perceive exogenous mechanical stress caused by environmental factors as well as endogenous mechanical stress, which is attributed to their own cell division and cellular growth (Hamant 2013; Sampathkumar 2020; Kouhen et al. 2023). Plant cell division depends on the balance between turgor pressure and cell wall resistance to tensile strength (Hamant and Haswell 2017). Plant cells and tissues are prestressed structures with high turgor pressure, which is 2- to 10-fold greater than the atmospheric pressure (Du and Jiao 2020; Long et al. 2020). Therefore, we speculated that MCAs could monitor not only exogenous mechanical stress but also endogenous mechanical stress to coordinate cell proliferation, differentiation, and morphogenesis throughout the life cycle to form the proper 3D architecture of plants. Cells constantly receive endogenous mechanical cues derived from the cell division and expansion of themselves or their neighbor cells during vegetative and reproductive growth and development. Thus, wild-type cells are considered to have responded to these stimuli to regulate $[\text{Ca}^{2+}]_{\text{cyt}}$ and divide normally. In contrast, the *Mpmca* mutant could not

respond to these endogenous mechanical stimuli, and $[Ca^{2+}]_{cyt}$ was lower than that of the wild type, resulting in a decrease in cell division activity. The adjustment of $[Ca^{2+}]_{cyt}$ by MpMCA under endogenous stress should be associated with the regulation of long-term $[Ca^{2+}]_{cyt}/Ca^{2+}$ homeostasis. Thus, our results suggest the possibility that MpMCA functions as a mechanosensitive channel that increases $[Ca^{2+}]_{cyt}$ in response to exogenous mechanical stress.

MpMCA might be related to lipid metabolism

TEM electron microscopy revealed the existence of a lipid body-like structure in the notch region of the dormant gemma. Lipid bodies are plant organelles that compartmentalize neutral lipids into a hydrophobic matrix covered by lipid body membrane proteins embedded in a phospholipid monolayer (Guzha et al. 2023). The major lipid-body-membrane protein families in seeds are oleosins, caleosins, and steroleosins, and neutral lipids are the source of carbon and energy for seed germination and growth (Guzha et al. 2023). Oleosins play important roles in regulating the biosynthesis, metabolism, and mobilization of lipids during seed maturation and germination (Parthibane et al. 2012). Caleosins contain a calcium-binding site, the EF-hand motif, at the N-terminus (Chen et al. 1999). Ca^{2+} and EF-hand are essential for the peroxidase activity of caleosins (Hanano et al. 2023). Some caleosins are also expressed in vegetative tissues and are induced by drought and osmotic stress in the leaves and stems (Aubert et al. 2010). Therefore, caleosins may be involved in the Ca^{2+} signaling pathway induced by drought stress. Lipid body-like structures in the notch region were rarely observed in *MpMCA* mutant or developing gemmae. Because caleosin-like genes are found in the *M. polymorpha* genome and MpMCA is required for the maintenance of $[Ca^{2+}]_{cyt}$ in the notch region (Fig. 2), MpMCA may regulate lipid body formation by regulating $[Ca^{2+}]_{cyt}$ and lipid metabolism.

The function of MCAs is widely conserved in land plants

The predicted MpMCA protein showed 39.5% and 38.7% amino acid sequence identity with AtMCA1 and AtMCA2, respectively (Fig. 1B). The approximately 170 amino acid (aa) N-terminal region containing a transmembrane region plus EF-hand-like domains ("MCA^{func}" domain: Nishii et al. 2021) was sufficient for Ca^{2+} permeation activity in vitro (Nakano et al. 2011). The sequence identity at this N-terminal region was higher than that in the full-length region between MpMCA and AtMCAs (54.4% and 50.9% with AtMCA1 and AtMCA2, respectively). AtMCA1, AtMCA2, NtMCA1, NtMCA2, and ZmMCA all exhibit the MCA (Nakagawa et al. 2007; Yamanaka et al. 2010; Kurusu et al. 2012b; Rosa et al. 2017).

In this study, we found that MpMCA was required for vegetative growth and sexual reproduction by regulating cell proliferation and differentiation. Our findings indicate that MpMCA modulates these phenomena by regulating $[Ca^{2+}]_{cyt}$ levels in the plasma membrane of actively dividing and differentiating cells. However, an in-depth understanding of the role of MCAs in regulating $[Ca^{2+}]_{cyt}$ to control cell proliferation and differentiation requires further biochemical and biophysical analyses of MpMCAs and other MCAs.

MpMCA has a conserved structural feature and activity in land plants

MpMCA is comprised of a single transmembrane segment, an EF hand-like motif in the N-terminal region, a coiled-coil motif in the middle, and a C-terminal PLAC8 motif (Nakagawa et al. 2007; Kamano et al. 2015). Although the sequence similarity of MCA^{func} domain with AtMCAs was higher than 50%, MpMCA lacks the

two amino acid residues, corresponding to the Leu²⁰/Ile²⁰ and Asp²¹ of AtMCA1 and AtMCA2, in the transmembrane region (Supplementary Fig. S7), which were shown to be involved in Ca^{2+} influx in Arabidopsis (Nakano et al. 2011; Yoshimura et al. 2021). In addition, MpMCA contains a Gln residue at a site corresponding to the Arg⁴⁴ of OsMCA1, which is essential for this channel's function (Liu et al. 2015) (Supplementary Fig. S7). Furthermore, no detectable Ca^{2+} transport activity of MpMCA was detected in the yeast *mid1 cch1* mutant. Nevertheless, MpMCA retained an ability to complement the yeast *mid1 cch1* mutant. More importantly, the *MpMCA* mutant showed traits similar to those observed in *mca* mutants of seed plants, such as defects in stress-induced increases in $[Ca^{2+}]_{cyt}$, plant growth and development, and cell proliferation. Finally, we demonstrated that AtMCA1 efficiently rescued defects in *MpMCA* mutant plants in both vegetative growth and sexual reproduction. Therefore, the common domain structure and basic function of MCAs could have already been established in the common ancestor of land plants before the ancestors of bryophytes and tracheophytes were separated, although the amino acid residues necessary for MCA function changed in a plant lineage-specific manner. Indeed, in the non-vascular plant lineages, hornworts, the MCA proteins contain Asp, but moss ones contain Asn at the corresponding position to Asp²¹ of MCA proteins.

Collectively, our results support that MpMCA is either a part of a mechanosensitive channel complex or that the presence of some species-specific molecules is required for mechanosensitive Ca^{2+} channel activity. To confirm the Ca^{2+} transport activity of MCAs, the electrophysiological and pharmacological analyses are essential. Furthermore, structural analysis of MpMCA and identification of in vivo interactors of MpMCA should help us reveal the role of MpMCA in the regulation of $[Ca^{2+}]_{cyt}$.

Materials and methods

Plant materials and growth conditions

The male and female *M. polymorpha* accessions, Takaragaike-1 (WT(M)) and Takaragaike-2 (WT(F)), respectively (Ishizaki et al. 2008), were used as wild type. Plants were grown on half-strength Gamborg's B5 medium (Gamborg et al. 1968) with or without 1% sugar containing 1% agar or on vermiculite supplemented with 1/2000-strength HYPONeX (Hyponex Japan, Osaka, Japan) under continuous white light from a cold cathode fluorescent lamp (50 to 60 $\mu\text{mol photons m}^{-2} \text{s}^{-1}$; OPT-40C-N-L., Oporom) at 22°C. To induce reproductive growth, 5-d-old gemmalings or older thalli were transferred to white-light conditions supplemented with FR (30 $\mu\text{mol photons m}^{-2} \text{s}^{-1}$, VBL-TFL600-IR730*, Valore, Kyoto, Japan). F₁ spores were generated by crossing Takaragaike-1 and Takaragaike-2 and used for the transformation of sporelings.

Plasmid construction, transformation, and selection of transformants

Oligo DNAs used in this study are listed in Supplementary Table S1.

To generate *proMpMCA:GUS* or *proMpMCA:Citrine-NLS*, the 5067 bp promoter sequence of MpMCA was amplified from wild-type genomic DNA with the primer pair MpMCA_{pro_FW1}/MpMCA_{pro_RV1} and cloned into the pENTR/D-TOPO entry vector (Thermo Fisher Scientific). Then, the cloned sequence was transferred to pMpGWB104 or pMpGWB115, respectively (Ishizaki et al. 2015), with LR Clonase II (Thermo Fisher Scientific).

To generate pMpGWB301_*proMpMCA*, pMpGWB301 was digested with *Xba*I and then the promoter sequence of MpMCA was amplified

from MpMCApro/pENTR with the primer pair MpMCApro_FW2/MpMCApro_RV2. The *proMpmca* PCR fragment was inserted into the *Xba*I site of pMpGWB301. To generate pENTR/D-TOPO_MpMCA, MpMCA cDNA was amplified from an *M. polymorpha* cDNA library with the primer pair MpMCA_F1/MpMCA_F2 and cloned into the pENTR/D-TOPO entry vector.

To obtain the plants expressing yellow cameleon 3.60 (YC3.60), YC3.60 coding sequence, which was codon optimized for Arabidopsis, was amplified with the primer pair YC3.60_FW/YC3.60_RV, and cloned into the pENTR/D-TOPO entry vector. The cloned sequence was transferred to pMpGWB301_*proMpmca* or pMpGWB103 with LR Clonase II to generate *proMpmca*:YC3.60 or *proMpef*:YC3.60, which were introduced into F1 sporelings by *Agrobacterium*-mediated transformation (Ishizaki et al. 2008). After transformation, we selected thalli emitting bright fluorescence from the plants growing on the agar plates containing hygromycin or chlorosulfuron using a fluorescent stereomicroscope (SMZ18, Nikon).

To obtain knockout lines of MpMCA, the gRNA oligo DNA sets (MpMCA_gRNAI_FW and MpMCA_gRNAI_RV for gRNAI; MpMCA_gRNAII_FW and MpMCA_gRNAII_RV for gRNAII) were annealed and then ligated into *Bsa*I-digested pMpGE_En03 vector (Sugano et al. 2018). The resulting constructs were transferred to the pMpGE010 or pMpGE011 binary vector (Sugano et al. 2018) to generate pMpGE010_MpMCA_gRNAI, pMpGE011_MpMCA_gRNAI, and pMpGE010_MpMCA_gRNAII. These constructs were introduced into F1 sporelings or regenerating thalli of *proMpmca*:YC3.60 or *proMpef*:YC3.60 expressing plants via *Agrobacterium* (Kubota et al. 2013). In order to isolate *Mpmca* mutants, the gRNAI- or gRNAII-targeted regions (Supplementary data S4) was amplified with genomic DNAs prepared from transformed thalli using the primer pair MpMCA_FW2/MpMCA_RV2. PCR products were directly sequenced with BigDye Terminator v3.1 (Thermo Fisher Scientific).

To obtain complementation lines in *Mpmca* (gRNAI) mutant background, MpMCA cDNA with synonymous substitutions that confer resistance to MpMCA_gRNAI (Supplementary data S4A), were made. First, by using the *Xho*I fragment containing gRNAI-target region (496 bp) from pENTR/D-TOPO_MpMCA as a template, two PCR fragments that were overlapped at the gRNAI target site and carried the synonymous substitutions were amplified with the primer sets; MpMCA_Xho1_FW/MpMCA_G1_comp_RV and MpMCA_G1_comp_FW/MpMCA_Xho1_RV. Then, using two resulting DNA fragments as templates, the *Xho*I fragment containing gRNAI-synonymous substitution were amplified by overlap extension PCR with the primer pair MpMCA_Xho1_FW/MpMCA_Xho1_RV. The resulting fragment was then inserted into *Xho*I site of pENTR/D-TOPO_MpMCA and then transferred into pMpGWB301_*proMpmca* with LR reaction to generate pMpGWB301_*proMpmca*: MpMCAcomp. The resulting complementation vector was introduced into regenerating thalli of *Mpmca* (gRNAI) plants via *Agrobacterium* (Kubota et al. 2013).

To obtain complementation lines expressing *mNeonGreen* in *Mpmca* (gRNAI) mutant background, MpMCAcomp without stop codon was fused with *mNeonGreen*, which was amplified from the enhanced Nano-lantern (eNL) (Suzuki et al. 2016) with the primer pair mNG_FW/mNG_RV. The PCR fragment was cloned into the pENTR/D-TOPO entry vector (MpMCAcomp_mNeonGreen) and then transferred into pMpGWB301_*proMpmca* with LR reaction to generate pMpGWB301_*proMpmca*: MpMCAcomp_mNeonGreen.

To obtain complementation lines in *proMpmca*:YC3.60-expressing *Mpmca* (gRNAI) mutant background, crossing with complementation lines expressing MpMCA cDNA with CRISPR/Cas9-resistant synonymous mutations was done and *Mpmca* lines expressing both *proMpmca*:YC3.60 and *proMpmca*: MpMCAcomp were selected.

To obtain *Mpmca* (gRNAI) mutant lines expressing AtMCA1, AtMCA1 cDNA was amplified from an Arabidopsis cDNA library (Fujita et al. 2003) with a primer pair AtMCA1_FW/AtMCA1_RV and cloned into pENTR/D-TOPO. The cloned sequence was then transferred to pMpGWB301_*proMpmca* with LR reaction to generate pMpGWB301_*proMpmca*:AtMCA1. The binary vector was introduced into regenerating thalli of *Mpmca* (gRNAI) plants via *Agrobacterium*.

GUS staining

For detection of GUS activity in situ, samples were incubated for from 6 to 18 h at 37°C in X-Gluc solution (2 mM 5-bromo-4-chloro-3-indolyl β -D-glucuronic acid, 50 mM sodium phosphate buffer, pH 7.0), and then washed with 70% to 100% ethanol (v/v) three or four times in order to remove chlorophyll. The images were obtained using a stereomicroscope (SMZ18, Nikon) or a digital camera (EOS Kiss X90, Canon).

Fluorescent imaging

For fluorescent imaging (Fig. 1), the samples were illuminated with blue green excitation light for Citrine and the images were obtained using a 535/40 emission filter with an inverted microscope (Axio Observer, Zeiss). For fluorescent imaging (Fig. 5D), the samples were excited with 514 nm laser for Citrine fluorescence or with 670 nm for chloroplast autofluorescence and the images were obtained in the range of 519 to 586 nm or 654 to 779 nm with confocal laser scanning microscopy (LSM) (TCS SP8 X FALCON; Leica Microsystems). For fluorescent imaging (Fig. 5I), the samples were excited with 491 nm laser for mNeonGreen fluorescence with LSM.

Ca²⁺ imaging system

For FRET imaging, the YC3.60-expression samples were imaged with a Zeiss inverted microscope (Axio Observer, ZEISS) equipped with a LED light (Prizmatrix), an EM-CCD Evolve 512 camera (Photometrics), and a filter exchanging system (Prior). The samples were illuminated with blue excitation light (438/24–25) for YC3.60, and imaging of the YC3.60 emission ratio was accomplished using two emission filters (483/32 for CFP, 535/40 for cpVenus). The FRET (cpVenus/CFP) ratio was determined using MetaMorph software (Molecular Devices, USA). A 10 \times /0.5 or a 20 \times /0.8 objective lens was used for imaging. Exposure times were 50 to 500 ms, and images were collected every 1 s to 5 min. In each experiment, the ratio in a region of interest was measured using the MetaMorph software, and it is shown as sequential line graphs. The mean and maximum values were calculated using Microsoft Excel.

For hydration and germination experiments, gemmae were mounted on the medium containing half-strength Gamborg's B5 medium without 1% sucrose and 1% agar (ultralow gelling temperature type IX-A) in moistened glass-bottomed dishes. For the hyperosmotic stress experiment, 8-d-old gemmalings were mounted on the glass-bottomed dish and covered with a small amount of half-strength Gamborg's B5 medium without 1% sucrose. Finally, half-strength Gamborg's B5 medium containing 0.4 M mannitol was added to a final concentration of 200 mM.

Functional characterization of MpMCA in yeast cells

The MpMCA cDNA sequence (MpMCA) was cloned into the YEplac181-based expression vector pBET that carries the yeast TDH3 promoter. Cells of yeast (*S. cerevisiae*) mutant strain H319 (MATa *mid1- Δ 5::HIS3 cch1 Δ ::HIS3*) expressing untagged MpMCA, FLAG-tagged MpMCA (MpMCA-FL), AtMCA1-FL, and AtMCA2-FL

were cultured at 30°C in SD.Ca100 medium containing the mating pheromone α -factor, as described previously (Nakano et al. 2011). The parental strain H207 (MATa MID1⁺ CCH1⁺) bearing the empty vector was used as a positive control. Before the following experiments, we selected yeast strains that express the same amount of MCA protein as each other. For viability assays, the above cultures were incubated for 8 h, and the cells were stained with methylene blue (MB). MB-negative (viable) and MB-positive (nonviable) cells were then counted, and the percentage (%) of cell viability was calculated (Iida et al. 1994; Nakagawa et al. 2007). For Ca²⁺ uptake assays, the above cultures were incubated for 2 h with ⁴⁵CaCl₂, after which ⁴⁵Ca²⁺ accumulation into the cells was measured, as described previously (Iida et al. 1994; Nakagawa et al. 2007).

The yeast complementation assays, using the *S. cerevisiae* mutant strain K667 (*crib1::LEU2 pmc1::TRP1 vcx1Δ*) (Cunningham and Fink 1996), was performed as described previously (Pittman and Hirschi 2001). The MpMCA cDNA sequence (MpMCA) or AtMCA1 was cloned into the yeast expression vector pYES2 that carries the URA3 gene as a selection marker and the GAL1 promoter. pYES2::MpMCA, pYES2::AtMCA1, and pYES2 empty vectors were introduced into K667 cells by the LiAc/carrier ssDNA/PEG method (Gietz and Schiestl 2007). Transformants were selected on synthetic complete (SC)-agar medium depleted of uracil (Yadav et al. 2015). Growth test assays were performed for the transformants grown for 5 to 8 d on SC-agar medium containing 2% agar, 2% galactose, and 1 (as the control), 50, 100, 125, or 150 mM CaCl₂ (high Ca²⁺).

Visualization of S-phase cells

S-phase cells were visualized with a Click-iT EdU Imaging Kit (Thermo Fisher Scientific) as described previously (Nishihama et al. 2015; Ishida et al. 2022; Shinkawa et al. 2022). For EdU assay on wild type, *Mpmca*, and *MpMCAcomp*, 3- or 7-d-old gemmalings were incubated with 10 μM EdU for 4 h. Incorporation of EdU was terminated by fixing explants with 3.7% formaldehyde solution in phosphate-buffered saline (PBS) for 1 h. After permeabilization with 0.5% Triton X-100 in PBS for 20 min, EdU incorporated into DNA was stained by incubation in the dark with Alexa Fluor 488-containing Click-iT reaction cocktail for 1 h. After washing with PBS containing 3% bovine serum albumin (BSA) and then PBS without BSA, the sample was treated with the clearing agent (Kurihara et al. 2015). Fluorescence excited by 491 nm laser was captured in a range of 498 to 573 nm with LSM or an all-in-one fluorescence microscope (BZ-X700, Keyence). For quantitative analysis of EdU-positive nucleus in 3-d-old gemmalings, Z-series of fluorescence images with 2 μm steps were captured and EDU-positive nuclei were counted manually.

LM and electron microscopy for morphological analysis

Sample preparation was performed as described previously (Koide et al. 2020). Briefly, the plant materials were fixed with 2.5% (v/v) glutaraldehyde and 2% (w/v) paraformaldehyde in 50 mM phosphate buffer pH7.2 (PB) at 4°C for more than 3 h. After washing with 50 mM PB, the samples were post-fixed with 2% (w/v) osmium tetroxide at room temperatures for 2 h. Then, fixed samples were washed three times with 8% (w/v) sucrose solution for 30 min, dehydrated in a graded series of ethanol, and embedded in epoxy resin (Quetol 812; Nisshin EM, Tokyo, Japan). For LM, semi-thin sections were cut with a diamond knife using an ultramicrotome (EM-UC6; Leica, Wetzlar Germany), mounted on microscope-slides, and stained with 1% (w/v) toluidine blue. Samples were observed with an LM (Axiophoto; Zeiss). For transmission electron microscopic

observation, ultra-thin sections (80 nm thick) were cut with a diamond knife using an ultramicrotome (EM-UC6; Leica, Wetzlar, Germany), mounted on a one-hole grid with supporting film, and stained with 2% (w/v) uranyl acetate and a lead stain solution. Samples were observed with TEM (H-7650; Hitachi, Japan) at 80 kV. For field emission scanning electron microscopic (FE-SEM) observation, serial sections (400 nm thick) were cut with a diamond knife using an ultramicrotome (EM-UC6; Leica, Wetzlar, Germany), mounted on a silicon wafer (380 μm thick; Canosis, Tokyo, Japan) and stained with 2% (w/v) uranyl acetate and a lead stain solution. Samples were observed with FE-SEM (JSM-7900F; JEOL, Tokyo, Japan). Images were obtained at 4 kV. Stacked images were aligned using the software (Stacker NEO; JEOL, Tokyo, Japan).

RNA extraction and RT-qPCR

To examine the expression level of MpCYCD;1, total RNA was extracted from the whole body of 3-d-old gemmalings grown under continuous white light. RNA extraction and RT-qPCR were performed as described previously (Ishida et al. 2022). MpEF1 was used as internal control for the normalization of the PCR. Primer pairs used for each gene are shown in Supplementary Table S2.

Statistical analysis

Statistical analysis was performed with GraphPad Prism software Ver. 9.5.0. For the comparison between two groups, an unpaired two-tailed t-test was used. For the multigroup comparison, a one-way analysis of variance (ANOVA) followed by Tukey's multiple comparison test was done. For comparison of one control group with all other group, a one-way ANOVA followed by Dunnett's multiple comparison test was done. The data were expressed as mean ± SD. Significance was defined at asterisks (*P < 0.05; **P < 0.01; ***P < 0.001; ****P < 0.0001) or letters.

Accession numbers

Sequence data from this article can be found in the GenBank/EMBL data libraries under accession numbers BFI36503.1.

Marchantia polymorpha gene sequence data from this research can be found in the MarpolBase (<https://marchantia.info>) with Mp5g19510/Mapoly0134s0009.

Acknowledgments

The authors thank Yoshihiro Yoshitake and Shohei Yamaoka for technical advice for vector construction; Atsushi Miyawaki in RIKEN for the supply of yellow cameleon 3.60/pRSET_B; Keiko Okamoto-Furuta, Haruyasu Kohda, Yasuko Koumoto, and Tomoo Shimada for the use of electron microscopy; Yukiko Yasui, Yoriko Matsuda, Chikako Inoue, and Miki Kioka for the supporting this research. This work was supported by Kyoto University Live Imaging Center.

Author contributions

Conceptualization, M.I., N.S., and T.Ko.; Resources, M.I., N.S., T.H., A.C., H.I., T.N., and T.Ko.; Investigation, M.I., N.S., S.I., T.Ka., T.H., M.K., and K.I.; Writing, M.I., and N.S. with input from all authors.

Supplementary data

The following materials are available in the online version of this article.

Supplementary Figure S1. Chromatic expression images of MpMCA (Mp5g19510) from public *M. polymorpha* transcriptome data at MarpolBase Expression (MBEX, <https://marchantia.info/mbex/>)

Supplementary Figure S2. Sequences of the MpMCA gene in Mpmca mutant lines generated by CRISPR/Cas9.

Supplementary Figure S3. Phenotype of two allele Mpmca expressing proMpMCA:YC3.60.

Supplementary Figure S4. Phenotype of Mpmca-1^{9e}(F) expressing proMpMCA:MpMCAcomp_mNeonGreen.

Supplementary Figure S5. Yeast *mid1* complementation experiments.

Supplementary Figure S6. Yeast K667 mutant complementation experiments.

Supplementary Figure S7. Amino acid sequence alignment of the N-terminal region of MpMCA, AtMCA1, AtMCA2, NtMCA1, NtMCA2, ZmMCA, and OsMCA1.

Supplementary Table S1. The list of primer sequences used for plasmid constructions.

Supplementary Table S2. The list of gene-specific RT-qPCR primer sequences.

Supplementary Video S1. [Ca²⁺]_{cyt} changes during just after gemma hydration to germination in wild type expressing proEF:YC3.60.

Supplementary Video S2. [Ca²⁺]_{cyt} changes during just after gemma hydration to germination in Mpmca expressing proEF:YC3.60.

Supplementary Video S3. [Ca²⁺]_{cyt} change induced by osmotic stress at the notch of wild type expressing proEF:YC3.60.

Supplementary Video S4. [Ca²⁺]_{cyt} change induced by osmotic stress at the notch of Mpmca expressing proEF:YC3.60.

Funding

This work was supported by JSPS KAKENHI Grant Numbers [JP20K06704 and JP23K05816 to M.I.; JP23K05711 to H.I.; JP17H07424 and JP22H00417 to T.K.; JP22K19304 to N.S.]. N.S. was also supported by funding from the Sumitomo Foundation Grand Number 210145, the TOREY Science Foundation Grant Number 21-6204, and the Yamada Science Foundation.

Conflict of interest statement. None declared.

Data availability

The data underlying this article are available in the article and in its online supplementary material.

References

- Althoff F, Kopsischke S, Zobell O, Ide K, Ishizaki K, Kohchi T, Zachgo S. Comparison of the MpEF1 α and CaMV35 promoters for application in *Marchantia polymorpha* overexpression studies. *Transgenic Res.* 2014;23(2):235–244. <https://doi.org/10.1007/s11248-013-9746-z>
- Aubert Y, Vile D, Pervent M, Aldon D, Ranty B, Simonneau T, Vavasseur A, Galaud JP. RD20, a stress-inducible caleosin, participates in stomatal control, transpiration and drought tolerance in *Arabidopsis thaliana*. *Plant Cell Physiol.* 2010;51(12):1975–1987. <https://doi.org/10.1093/pcp/pcq155>
- Berridge MJ, Lipp P, Bootman MD. The versatility and universality of calcium signalling. *Nat Rev Mol Cell Biol.* 2000;1(1):11–21. <https://doi.org/10.1038/35036035>
- Bowman JL, Arteaga-Vazquez M, Berger F, Briginshaw LN, Carella P, Aguilar-Cruz A, Davies KM, Dierschke T, Dolan L, Dorantes-Acosta AE, et al. The renaissance and enlightenment of *Marchantia* as a model system. *Plant Cell.* 2022;34(10):3512–3542. <https://doi.org/10.1093/plcell/koac219>
- Chen J, Gutjahr C, Bleckmann A, Dresselhaus T. Calcium signaling during reproduction and biotrophic fungal interactions in plants. *Mol Plant.* 2015;8(4):595–611. <https://doi.org/10.1016/j.molp.2015.01.023>
- Chen JCF, Tsai CCY, Tzen JTC. Cloning and secondary structure analysis of caleosin, a unique calcium-binding protein in oil bodies of plant seeds. *Plant Cell Physiol.* 1999;40(10):1079–1086. <https://doi.org/10.1093/oxfordjournals.pcp.a029490>
- Chiyoda S, Ishizaki K, Kataoka H, Yamato KT, Kohchi T. Direct transformation of the liverwort *Marchantia polymorpha* L. by particle bombardment using immature thalli developing from spores. *Plant Cell Rep.* 2008;27(9):1467–1473. <https://doi.org/10.1007/s00299-008-0570-5>
- Cunningham KW, Fink GR. Calcineurin inhibits VCX1-dependent H⁺/Ca²⁺ exchange and induces Ca²⁺ ATPases in *Saccharomyces cerevisiae*. *Mol Cell Biol.* 1996;16(5):2226–2237. <https://doi.org/10.1128/MCB.16.5.2226>
- Du F, Jiao Y. Mechanical control of plant morphogenesis: concepts and progress. *Curr Opin Plant Biol.* 2020;57:16–23. <https://doi.org/10.1016/j.pbi.2020.05.008>
- Edel KH, Marchadier E, Brownlee C, Kudla J, Hetherington AM. The evolution of calcium-based signalling in plants. *Curr Biol.* 2017;27(13):R667–R679. <https://doi.org/10.1016/j.cub.2017.05.020>
- Engelsdorf T, Gigli-Bisceglia N, Veerabagu M, McKenna JF, Vaahtera L, Augstein F, Van der Does D, Zipfel C, Hamann T. The plant cell wall integrity maintenance and immune signaling systems cooperate to control stress responses in *Arabidopsis thaliana*. *Sci Signal.* 2018;11(536):eaao3070. <https://doi.org/10.1126/scisignal.aao3070>
- Fujita H, Takemura M, Tani E, Nemoto K, Yokota A, Kohchi T. An *Arabidopsis* MADS-box protein, AGL24, is specifically bound to and phosphorylated by meristematic receptor-like kinase (MRLK). *Plant Cell Physiol.* 2003;44(7):735–742. <https://doi.org/10.1093/pcp/pcg092>
- Furuichi T, Cunningham KW, Muto S. A putative two pore channel AtTPC1 mediates Ca²⁺ flux in *Arabidopsis* leaf cells. *Plant Cell Physiol.* 2001;42(9):900–905. <https://doi.org/10.1093/pcp/pce145>
- Furuichi T, Iida H, Sokabe M, Tatsumi H. Expression of *Arabidopsis* MCA1 enhanced mechanosensitive channel activity in the *Xenopus laevis* oocyte plasma membrane. *Plant Signal Behav.* 2012;7(8):1022–1026. <https://doi.org/10.4161/psb.20783>
- Gamborg OL, Miller RA, Ojima K. Nutrient requirements of suspension cultures of soybean root cells. *Exp Cell Res.* 1968;50(1):151–158. [https://doi.org/10.1016/0014-4827\(68\)90403-5](https://doi.org/10.1016/0014-4827(68)90403-5)
- Gao QF, Gu LL, Wang HQ, Fei CF, Fang X, Hussain J, Sun SJ, Dong JY, Liu H, Wang YF. Cyclic nucleotide-gated channel 18 is an essential Ca²⁺ channel in pollen tube tips for pollen tube guidance to ovules in *Arabidopsis*. *Proc Natl Acad Sci U S A.* 2016;113(11):3096–3101. <https://doi.org/10.1073/pnas.1524629113>
- Gietz RD, Schiestl RH. High-efficiency yeast transformation using the LiAc/SS carrier DNA/PEG method. *Nat Protoc.* 2007;2(1):31–34. <https://doi.org/10.1038/nprot.2007.13>
- Grenzi M, Buratti S, Parmagnani AS, Abdel Aziz I, Bernacka-Wojcik I, Resentini F, Šimura J, Doccula FG, Alfieri A, Luoni L, et al. Long-distance turgor pressure changes induce local activation of plant glutamate receptor-like channels. *Curr Biol.* 2023;33(6):1019–1035.e8. <https://doi.org/10.1016/j.cub.2023.01.042>
- Grenzi M, Resentini F, Vanneste S, Zottini M, Bassi A, Costa A. Illuminating the hidden world of calcium ions in plants with a

- universe of indicators. *Plant Physiol.* 2021;187(2):550–571. <https://doi.org/10.1093/plphys/kiab339>
- Guichard M, Thomine S, Frachisse JM. Mechanotransduction in the spotlight of mechano-sensitive channels. *Curr Opin Plant Biol.* 2022;68:102252. <https://doi.org/10.1016/j.pbi.2022.102252>
- Guzha A, Whitehead P, Ischebeck T, Chapman KD. Lipid droplets: packing hydrophobic molecules within the aqueous cytoplasm. *Annu Rev Plant Biol.* 2023;74(1):195–223. <https://doi.org/10.1146/annurev-arplant-070122-021752>
- Hamant O. Widespread mechanosensing controls the structure behind the architecture in plants. *Curr Opin Plant Biol.* 2013;16(5):654–660. <https://doi.org/10.1016/j.pbi.2013.06.006>
- Hamant O, Haswell ES. Life behind the wall: sensing mechanical cues in plants. *BMC Biol.* 2017;15(1):59. <https://doi.org/10.1186/s12915-017-0403-5>
- Hamilton ES, Schlegel AM, Haswell ES. United in diversity: mechano-sensitive ion channels in plants. *Annu Rev Plant Biol.* 2015;66(1):113–137. <https://doi.org/10.1146/annurev-arplant-043014-114700>
- Hanano A, Blée E, Murphy DJ. Caleosin/peroxygenases: multifunctional proteins in plants. *Ann Bot.* 2023;131(3):387–409. <https://doi.org/10.1093/aob/mcad001>
- Hashimoto K, Koselski M, Tsuboyama S, Dziubinska H, Trębacz K, Kuchitsu K. Functional analyses of the two distinctive types of two-pore channels and the slow vacuolar channel in *Marchantia polymorpha*. *Plant Cell Physiol.* 2022;63(2):163–175. <https://doi.org/10.1093/pcp/pcab176>
- Hatada M, Akiyama R, Yamagishi M, Ishizaki K, Mizutani M. MpDWF5A-Encoded sterol $\Delta 7$ -reductase is essential for the normal growth and development of *Marchantia polymorpha*. *Plant Cell Physiol.* 2023;64(7):826–838. <https://doi.org/10.1093/pcp/pcad043>
- Hattori T, Otomi Y, Nakajima Y, Soga K, Wakabayashi K, Iida H, Hoson T. MCA1 and MCA2 are involved in the response to hypergravity in *Arabidopsis* hypocotyls. *Plants (Basel).* 2020;9(5):590. <https://doi.org/10.3390/plants9050590>
- Hepler PK. Calcium: a central regulator of plant growth and development. *Plant Cell.* 2005;17(8):2142–2155. <https://doi.org/10.1105/tpc.105.032508>
- Higo A, Niwa M, Yamato KT, Yamada L, Sawada H, Sakamoto T, Kurata T, Shirakawa M, Endo M, Shigenobu S, et al. Transcriptional framework of male gametogenesis in the liverwort *Marchantia polymorpha* L. *Plant Cell Physiol.* 2016;57(2):325–338. <https://doi.org/10.1093/pcp/pcw005>
- Iida H, Nakamura H, Ono T, Okumura MS, Anraku Y. MID1, a novel *Saccharomyces cerevisiae* gene encoding a plasma membrane protein, is required for Ca^{2+} influx and mating. *Mol Cell Biol.* 1994;14(12):8259–8271. <https://doi.org/10.1128/mcb.14.12.8259-8271.1994>
- Ishida S, Suzuki H, Iwaki A, Kawamura S, Yamaoka S, Kojima M, Takebayashi Y, Yamaguchi K, Shigenobu S, Sakakibara H, et al. Diminished auxin signaling triggers cellular reprogramming by inducing a regeneration factor in the liverwort *Marchantia polymorpha*. *Plant Cell Physiol.* 2022;63(3):384–400. <https://doi.org/10.1093/pcp/pcac004>
- Ishizaki K, Chiyoda S, Yamato KT, Kohchi T. Agrobacterium-mediated transformation of the haploid liverwort *Marchantia polymorpha* L., an emerging model for plant biology. *Plant Cell Physiol.* 2008;49(7):1084–1091. <https://doi.org/10.1093/pcp/pcn085>
- Ishizaki K, Nishihama R, Ueda M, Inoue K, Ishida S, Nishimura Y, Shikanai T, Kohchi T. Development of gateway binary vector series with four different selection markers for the liverwort *Marchantia polymorpha*. *PLoS One.* 2015;10(9):e0138876. <https://doi.org/10.1371/journal.pone.0138876>
- Iwano M, Ito K, Fujii S, Kakita M, Asano-Shimosato H, Igarashi M, Kaothien-Nakayama P, Entani T, Kanatani A, Takehisa M, et al. Calcium signalling mediates self-incompatibility response in the Brassicaceae. *Nat Plants.* 2015;1(9):15128. <https://doi.org/10.1038/nplants.2015.128>
- Kamano S, Kume S, Iida K, Lei KJ, Nakano M, Nakayama Y, Iida H. Transmembrane topologies of Ca^{2+} -permeable mechanosensitive channels MCA1 and MCA2 in *Arabidopsis thaliana*. *J Biol Chem.* 2015;290(52):30901–30909. <https://doi.org/10.1074/jbc.M115.692574>
- Kanzaki M, Nagasawa M, Kojima I, Sato C, Naruse K, Sokabe M, Iida H. Molecular identification of a eukaryotic, stretch-activated nonselective cation channel. *Science.* 1999;285(5429):882–886. Erratum in: *Science* 1999;285(5433):1493. Erratum in: *Science*. 2000;288(5470):1347. <https://doi.org/10.1126/science.288.5470.1347>
- Kaplan B, Sherman T, Fromm H. Cyclic nucleotide-gated channels in plants. *FEBS Lett.* 2007;581(12):2237–2246. <https://doi.org/10.1016/j.febslet.2007.02.017>
- Kawamura S, Romani F, Yagura M, Mochizuki T, Sakamoto M, Yamaoka S, Nishihama R, Nakamura Y, Yamato KT, Bowman JL, et al. MarpolBase expression: a web-based, comprehensive platform for visualization and analysis of transcriptomes in the liverwort *Marchantia polymorpha*. *Plant Cell Physiol.* 2022;63(11):1745–1755. <https://doi.org/10.1093/pcp/pcac129>
- Kintzer AF, Stroud RM. Structure, inhibition and regulation of two-pore channel TPC1 from *Arabidopsis thaliana*. *Nature.* 2016;531(7593):258–262. <https://doi.org/10.1038/nature17194>
- Kohchi T, Yamato KT, Ishizaki K, Yamaoka S, Nishihama R. Development and molecular genetics of *Marchantia polymorpha*. *Annu Rev Plant Biol.* 2021;72(1):677–702. <https://doi.org/10.1146/annurev-arplant-082520-094256>
- Koide E, Suetsugu N, Iwano M, Gotoh E, Nomura Y, Stolze SC, Nakagami H, Kohchi T, Nishihama R. Regulation of photosynthetic carbohydrate metabolism by a Raf-like kinase in the liverwort *Marchantia polymorpha*. *Plant Cell Physiol.* 2020;61(3):631–643. <https://doi.org/10.1093/pcp/pcz232>
- Kouhen M, Dimitrova A, Scippa GS, Trupiano D. The course of mechanical stress: types, perception, and plant response. *Biology (Basel).* 2023;12(2):217. <https://doi.org/10.3390/biology12020217>
- Kubota A, Ishizaki K, Hosaka M, Kohchi T. Efficient Agrobacterium-mediated transformation of the liverwort *Marchantia polymorpha* using regenerating thalli. *Biosci Biotechnol Biochem.* 2013;77(1):167–1672. <https://doi.org/10.1271/bbb.120700>
- Kubota A, Kita S, Ishizaki K, Nishihama R, Yamato KT, Kohchi T. Co-option of a photoperiodic growth-phase transition system during land plant evolution. *Nat Commun.* 2014;5(1):3668. <https://doi.org/10.1038/ncomms4668>
- Kurihara D, Mizuta Y, Sato Y, Higashiyama T. ClearSee: a rapid optical clearing reagent for whole-plant fluorescence imaging. *Development.* 2015;142(23):4168–4179. <https://doi.org/10.1242/dev.127613>
- Kurusu T, Kuchitsu K, Nakano M, Nakayama Y, Iida H. Plant mechanosensing and Ca^{2+} transport. *Trends Plant Sci.* 2013;18(4):227–233. <https://doi.org/10.1016/j.tplants.2012.12.002>
- Kurusu T, Nishikawa D, Yamazaki Y, Gotoh M, Nakano M, Hamada H, Yamanaka T, Iida K, Nakagawa Y, Saji H, et al. Plasma membrane protein OsMCA1 is involved in regulation of hypo-osmotic shock-induced Ca^{2+} influx and modulates generation of reactive oxygen species in cultured rice cells. *BMC Plant Biol.* 2012a;12(1):11. <https://doi.org/10.1186/1471-2229-12-11>
- Kurusu T, Yamanaka T, Nakano M, Takiguchi A, Ogasawara Y, Hayashi T, Iida K, Hanamata S, Shinozaki K, Iida H, et al. Involvement of the putative Ca^{2+} -permeable mechanosensitive channels, NtMCA1 and NtMCA2, in Ca^{2+} uptake, Ca^{2+} -dependent cell proliferation and mechanical stress-induced gene expression

- in tobacco (*Nicotiana tabacum*) BY-2 cells. *J Plant Res.* 2012b;125(4):555–568. <https://doi.org/10.1007/s10265-011-0462-6>
- Liang J, He Y, Zhang Q, Wang W, Zhang Z. Plasma membrane Ca²⁺-permeable mechanosensitive channel OsDMT1 is involved in regulation of plant architecture and ion homeostasis in rice. *Int J Mol Sci.* 2020;21(3):1097. <https://doi.org/10.3390/ijms21031097>
- Liu Z, Cheng Q, Sun Y, Dai H, Song G, Guo Z, Qu X, Jiang D, Liu C, Wang W, et al. A SNP in OsMCA1 responding for a plant architecture defect by deactivation of bioactive GA in rice. *Plant Mol Biol.* 2015;87(1–2):17–30. <https://doi.org/10.1007/s11103-014-0257-y>
- Long Y, Cheddadi I, Mosca G, Mirabet V, Dumond M, Kiss A, Traas J, Godin C, Boudaoud A. Cellular heterogeneity in pressure and growth emerges from tissue topology and geometry. *Curr Biol.* 2020;30(8):1504–1516.e8. <https://doi.org/10.1016/j.cub.2020.02.027>
- Luan S, Wang C. Calcium signaling mechanisms across kingdoms. *Annu Rev Cell Dev Biol.* 2021;37(1):311–340. <https://doi.org/10.1146/annurev-cellbio-120219-035210>
- Lucca N, León G. Arabidopsis ACA7, encoding a putative auto-regulated Ca⁽²⁺⁾-ATPase, is required for normal pollen development. *Plant Cell Rep.* 2012;31(4):651–659. <https://doi.org/10.1007/s00299-011-1182-z>
- Marchetti F, Cainzos M, Cascallares M, Distéfano AM, Setzes N, López GA, Zabaleta E, Pagnussat GC. Heat stress in *Marchantia polymorpha*: sensing and mechanisms underlying a dynamic response. *Plant Cell Environ.* 2021;44(7):2134–2149. <https://doi.org/10.1111/pce.13914>
- Michard E, Lima PT, Borges F, Silva AC, Portes MT, Carvalho JE, Gilliam M, Liu LH, Obermeyer G, Feijó JA. Glutamate receptor-like genes form Ca²⁺ channels in pollen tubes and are regulated by pistil D-serine. *Science.* 2011;332(6028):434–437. <https://doi.org/10.1126/science.1201101>
- Miyata K, Hosotani M, Akamatsu A, Takeda N, Jiang W, Sugiyama T, Takaoka R, Matsumoto K, Abe S, Shibuya N, et al. OsSYMRK plays an essential role in AM symbiosis in rice (*Oryza sativa*). *Plant Cell Physiol.* 2023;64(4):378–391. <https://doi.org/10.1093/pcp/pcad006>
- Miyawaki A, Nagai T, Mizuno H. Imaging intracellular free Ca²⁺ concentration using yellow cameleons. *Cold Spring Harb Protoc.* 2013;2013(11):pdb.prot078642. <https://doi.org/10.1101/pdb.prot078642>
- Mori K, Renhu N, Naito M, Nakamura A, Shiba H, Yamamoto T, Suzuki T, Iida H, Miura K. Ca²⁺-permeable mechanosensitive channels MCA1 and MCA2 mediate cold-induced cytosolic Ca²⁺ increase and cold tolerance in Arabidopsis. *Sci Rep.* 2018;8(1):550. <https://doi.org/10.1038/s41598-017-17483-y>
- Mousavi SA, Chauvin A, Pascaud F, Kellenberger S, Farmer EE. GLUTAMATE RECEPTOR-LIKE genes mediate leaf-to-leaf wound signalling. *Nature.* 2013;500(7463):422–426. <https://doi.org/10.1038/nature12478>
- Mousavi SAR, Dubin AE, Zeng WZ, Coombs AM, Do K, Ghadiri DA, Keenan WT, Ge C, Zhao Y, Patapoutian A. PIEZO ion channel is required for root mechanotransduction in *Arabidopsis thaliana*. *Proc Natl Acad Sci U S A.* 2021;118(20):e2102188118. <https://doi.org/10.1073/pnas.2102188118>
- Nagai T, Yamada S, Tominaga T, Ichikawa M, Miyawaki A. Expanded dynamic range of fluorescent indicators for Ca⁽²⁺⁾ by circularly permuted yellow fluorescent proteins. *Proc Natl Acad Sci U S A.* 2004;101(29):10554–10559. <https://doi.org/10.1073/pnas.0400417101>
- Nakagawa Y, Katagiri T, Shinozaki K, Qi Z, Tatsumi H, Furuichi T, Kishigami A, Sokabe M, Kojima I, Sato S, et al. Arabidopsis plasma membrane protein crucial for Ca²⁺ influx and touch sensing in roots. *Proc Natl Acad Sci U S A.* 2007;104(9):3639–3644. <https://doi.org/10.1073/pnas.0607703104>
- Nakano M, Furuichi T, Sokabe M, Iida H, Tatsumi H. The gravistimulation-induced very slow Ca²⁺ increase in Arabidopsis seedlings requires MCA1, a Ca²⁺-permeable mechanosensitive channel. *Sci Rep.* 2021;11(1):227. <https://doi.org/10.1038/s41598-020-80733-z>
- Nakano M, Furuichi T, Sokabe M, Iida H, Yano S, Tatsumi H. Entanglement of Arabidopsis seedlings to a mesh substrate under microgravity conditions in KIBO on the ISS. *Plants (Basel).* 2022;11(7):956. <https://doi.org/10.3390/plants11070956>
- Nakano M, Iida K, Nyunoya H, Iida H. Determination of structural regions important for Ca²⁺ uptake activity in Arabidopsis MCA1 and MCA2 expressed in yeast. *Plant Cell Physiol.* 2011;52(11):1915–1930. <https://doi.org/10.1093/pcp/pcr131>
- Nishihama R, Ishizaki K, Hosaka M, Matsuda Y, Kubota A, Kohchi T. Phytochrome-mediated regulation of cell division and growth during regeneration and sporeling development in the liverwort *Marchantia polymorpha*. *J Plant Res.* 2015;128(3):407–421. <https://doi.org/10.1007/s10265-015-0724-9>
- Nishii K, Möller M, Iida H. Mix and match: patchwork domain evolution of the land plant-specific Ca²⁺-permeable mechanosensitive channel MCA. *PLoS One.* 2021;16(4):e0249735. <https://doi.org/10.1371/journal.pone.0249735>
- Okamoto T, Takatani S, Motose H, Iida H, Takahashi T. The root growth reduction in response to mechanical stress involves ethylene-mediated microtubule reorganization and transmembrane receptor-mediated signal transduction in Arabidopsis. *Plant Cell Rep.* 2021;40(3):575–582. <https://doi.org/10.1007/s00299-020-02653-6>
- Parthibane V, Rajakumari S, Venkateshwari V, Iyappan R, Rajasekharan R. Oleosin is bifunctional enzyme that has both monoacylglycerol acyltransferase and phospholipase activities. *J Biol Chem.* 2012;287(3):1946–1954. <https://doi.org/10.1074/jbc.M111.309955>
- Pittman JK, Hirschi KD. Regulation of CAX1, an Arabidopsis Ca⁽²⁺⁾/H⁺ antiporter. Identification of an N-terminal autoinhibitory domain. *Plant Physiol.* 2001;127(3):1020–1029. <https://doi.org/10.1104/pp.010409>
- Proust H, Honkanen S, Jones VA, Morieri G, Prescott H, Kelly S, Ishizaki K, Kohchi T, Dolan L. RSL Class I Genes Controlled the Development of Epidermal Structures in the Common Ancestor of Land Plants. *Curr Biol.* 2016;26(1):93–99. <https://doi.org/10.1016/j.cub.2015.11.042>
- Radin I, Richardson RA, Coomey JH, Weiner ER, Bascom CS, Li T, Bezanilla M, Haswell ES. Plant PIEZO homologs modulate vacuole morphology during tip growth. *Science.* 2021;373(6554):586–590. <https://doi.org/10.1126/science.abe6310>
- Rasmussen H. Cell communication, calcium ion, and cyclic adenosine monophosphate. *Science.* 1970;170(3956):404–412. <https://doi.org/10.1126/science.170.3956.404>
- Resentini F, Ruberti C, Grenzi M, Bonza MC, Costa A. The signatures of organellar calcium. *Plant Physiol.* 2021;187(4):1985–2004. <https://doi.org/10.1093/plphys/kiab189>
- Rosa M, Abraham-Juárez MJ, Lewis MW, Fonseca JP, Tian W, Ramirez V, Luan S, Pauly M, Hake S. The maize MID-COMPLEMENTING ACTIVITY homolog CELL NUMBER REGULATOR13/NARROW ODD DWARF coordinates organ growth and tissue patterning. *Plant Cell.* 2017;29(3):474–490. <https://doi.org/10.1105/tpc.16.00878>
- Sampathkumar A. Mechanical feedback-loop regulation of morphogenesis in plants. *Development.* 2020;147(16):dev177964. <https://doi.org/10.1242/dev.177964>
- Schiøtt M, Romanowsky SM, Baekgaard L, Jakobsen MK, Palmgren MG, Harper JF. A plant plasma membrane Ca²⁺ pump is required for normal pollen tube growth and fertilization. *Proc Natl Acad Sci U S A.* 2004;101(25):9502–9507. <https://doi.org/10.1073/pnas.0401542101>
- Shigematsu H, Iida K, Nakano M, Chaudhuri P, Iida H, Nagayama K. Structural characterization of the mechanosensitive channel

- candidate MCA2 from *Arabidopsis thaliana*. *PLoS One*. 2014;9(1):e87724. <https://doi.org/10.1371/journal.pone.0087724>
- Shinkawa H, Kajikawa M, Furuya T, Nishihama R, Tsukaya H, Kohchi T, Fukuzawa H. Protein kinase MpYAK1 is involved in meristematic cell proliferation, reproductive phase change and nutrient signaling in the liverwort *Marchantia polymorpha*. *Plant Cell Physiol*. 2022;63(8):1063–1077. <https://doi.org/10.1093/pcp/pcac076>
- Simon AA, Navarro-Retamal C, Feijó JA. Merging signaling with structure: functions and mechanisms of plant glutamate receptor ion channels. *Annu Rev Plant Biol*. 2023;74(1):415–452. <https://doi.org/10.1146/annurev-arplant-070522-033255>
- Sugano SS, Nishihama R, Shirakawa M, Takagi J, Matsuda Y, Ishida S, Shimada T, Hara-Nishimura I, Osakabe K, Kohchi T. Efficient CRISPR/Cas9-based genome editing and its application to conditional genetic analysis in *Marchantia polymorpha*. *PLoS One*. 2018;13(10):e0205117. <https://doi.org/10.1371/journal.pone.0205117>
- Suzuki K, Kimura T, Shinoda H, Bai G, Daniels MJ, Arai Y, Nakano M, Nagai T. Five colour variants of bright luminescent protein for real-time multicolour bioimaging. *Nat Commun*. 2016;7(1):13718. <https://doi.org/10.1038/ncomms13718>
- Tian W, Hou C, Ren Z, Wang C, Zhao F, Dahlbeck D, Hu S, Zhang L, Niu Q, Li L, et al. A calmodulin-gated calcium channel links pathogen patterns to plant immunity. *Nature*. 2019;572(7767):131–135. <https://doi.org/10.1038/s41586-019-1413-y>
- Toyooka K, Goto Y, Hashimoto K, Wakazaki M, Sato M, Hirai MY. Endoplasmic reticulum bodies in the lateral root cap are involved in the direct transport of beta-glucosidase to vacuoles. *Plant Cell Physiol*. 2023;64(5):461–473. <https://doi.org/10.1093/pcp/pcac177>
- Toyota M, Spencer D, Sawai-Toyota S, Jiaqi W, Zhang T, Koo AJ, Howe GA, Gilroy S. Glutamate triggers long-distance, calcium-based plant defense signaling. *Science*. 2018;361(6407):1112–1115. <https://doi.org/10.1126/science.aat7744>
- Tse SW, Annese D, Romani F, Guzman-Chavez F, Bonter I, Forestier E, Frangedakis E, Haseloff J. Optimizing promoters and subcellular localization for constitutive transgene expression in *Marchantia polymorpha*. *Plant Cell Physiol*. 2024;65(8):1298–1309. <https://doi.org/10.1093/pcp/pcac063>
- Varshney K, Gutjahr C. KAI2 can do: Karrikin receptor function in plant development and response to abiotic and biotic factors. *Plant Cell Physiol*. 2023;64(9):984–995. <https://doi.org/10.1093/pcp/pcad077>
- Watanabe K, Hashimoto K, Hasegawa K, Shindo H, Tsuruda Y, Kupisz K, Koselski M, Wasko P, Trebacz K, Kuchitsu K. Rapid propagation of Ca²⁺ waves and electrical signals in a liverwort *Marchantia polymorpha*. *Plant Cell Physiol*. 2024;65(4):660–670. <https://doi.org/10.1093/pcp/pcad159>
- Wu X, Yuan F, Wang X, Zhu S, Pei ZM. Evolution of osmosensing OSCA1 Ca²⁺ channel family coincident with plant transition from water to land. *Plant Genome*. 2022;15(2):e20198. <https://doi.org/10.1002/tpg2.20198>
- Yadav AK, Shankar A, Jha SK, Kanwar P, Pandey A, Pandey GK. A rice tonoplast calcium exchanger, OsCCX2 mediates Ca²⁺/cation transport in yeast. *Sci Rep*. 2015;5(1):17117. <https://doi.org/10.1038/srep17117>
- Yamanaka T, Nakagawa Y, Mori K, Nakano M, Imamura T, Kataoka H, Terashima A, Iida K, Kojima I, Katagiri T, et al. MCA1 and MCA2 that mediate Ca²⁺ uptake have distinct and overlapping roles in *Arabidopsis*. *Plant Physiol*. 2010;152(3):1284–1296. <https://doi.org/10.1104/pp.109.147371>
- Yamaoka S, Nishihama R, Yoshitake Y, Ishida S, Inoue K, Saito M, Okahashi K, Bao H, Nishida H, Yamaguchi K, et al. Generative cell specification requires transcription factors evolutionarily conserved in land plants. *Curr Biol*. 2018;28(3):479–486.e5. <https://doi.org/10.1016/j.cub.2017.12.053>
- Yoshimura K, Iida K, Iida H. MCAs in *Arabidopsis* are Ca²⁺-permeable mechanosensitive channels inherently sensitive to membrane tension. *Nat Commun*. 2021;12(1):6074. <https://doi.org/10.1038/s41467-021-26363-z>
- Yuan F, Yang H, Xue Y, Kong D, Ye R, Li C, Zhang J, Theprungsirikul L, Shrift T, Krichilsky B, et al. OSCA1 mediates osmotic-stress-evoked Ca²⁺ increases vital for osmosensing in *Arabidopsis*. *Nature*. 2014;514(7522):367–371. <https://doi.org/10.1038/nature13593>